ACS OMEGA

Open Access



http://pubs.acs.org/journal/acsodf

Article

# Retardation of the C-Steel Destruction in Hydrochloric Acid Media Utilizing an Effective Schiff Base Inhibitor: Experimental and Theoretical Computations

Mahmoud G. Aboubakr Saleh,* Majda Alfakeer,* Rasha N. Felaly, Merfat S. Al-Sharif, Salih S. Al-Juaid, Kamal A. Soliman, Mohamed A. Hegazy, Sameer Nooh, Metwally Abdallah, and Salah Abd El Wanees*

Cite This: *ACS Omega* 2024, 9, 29666−29681

Read Online

ACCESS | Metrics & More | Article Recommendations

**ABSTRACT:** The corrosion inhibition of $(N^1E)$-$N^1$,$N^2$-bis(4-(dimethylamino)benzylidene)-ethane-1,2-diamine, DMAB, against the destruction of C-steel in dilute HCl media (1.0 M) was examined. The techniques of gravimetry, gasometry, potentiodynamic, and electrochemical impedance spectroscopy are utilized. The rate of corrosion is found to decrease with more additions of the DMAB compound. The inhibition efficacy increases with concentrations to reach 97.7% at 5.0 mM and 298 K. The protection of metal destruction is controlled by the adsorption of the DMAB molecules on the metallic surface obeying Langmuir's pattern. The computed $\Delta G^{\circ}_{ads}$ values are characterized by negative sign, explaining the spontaneity of the adsorption process. These values vary between −38.70 and −35.13 kJ mol$^{-1}$ depending on the temperature, which proves the physio- and chemisorption mechanisms. The reduction in $K_{ads}$ values with $T$ can be attributed to the desorption of some DMAB molecules from the electrode surface. Theoretical quantum computation confirms the adsorption of the DMAB compound in concurrence with the data obtained by practical techniques.

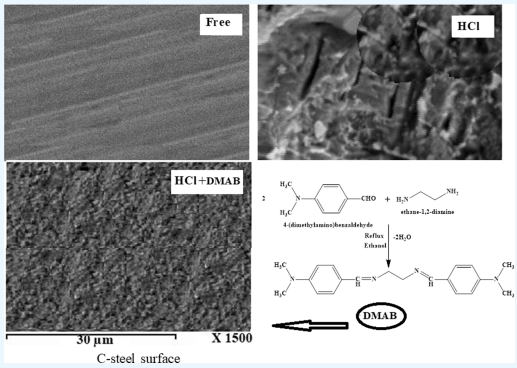


## 1. INTRODUCTION

Carbon steel (C-steel) pipes are fundamental to use in oil and gas applications. The drastic uses of C-steel are linked with its immoderate utilization in various industrial applications as a result of its reputable mechanical properties in addition to the relatively low production cost.[1,2] It is known that mineral acids are generally utilized to remove metallic sediments and rust in various industrial processes. HCl solutions are extremely utilized in the metal pickling processes. The harmful usage of inorganic acids is the damaging impact of such acids on the investigated metal, which causes a loss of metallic wealth.[3] Safe, environmentally friendly organic compounds are widely used these days to reduce corrosion processes and withstand the deleterious effect of such acids against metallic surfaces.[4] The selection of an inhibitor for retardation of corrosion of metals can rely primarily on its economic uses and the existence of heteroatoms like nitrogen or oxygen atoms in between its molecular formula that should be safe and eco-friendly compounds without leaving harmful effects.[5−12]

Schiff base comprising a carbon−nitrogen double bond azomethine functional group synthesized from a dehydration reaction between a keto aromatic and amine compounds has been shown to expand more inhibition execution compared with the related amines.[13] The inhibition performance of such compounds was found to rely on the presence of heteroatoms that are considered active adsorption centers that can introduce electron pairs to the investigated metallic surface. 4-Amino-*N*-benzylidene-benzamide was utilized as a general mitigator to reduce the damaging effect of dilute hydrochloric acid media on the steel with a protection efficacy of 79% at a concentration of 10 mM.[14] Betti et al. utilized ((5-mercapto-1,3,4-thiadiazol-2-yl)imino)indolin-2-one as a cutting-edge inhibitor to inhibit the corrosion of mild steel in 1.0 M HCl solution. The data of the chemical and electrochemical measurements confirmed that the protection efficiency reached 96.7% at a concentration of 0.5 mM at 303 K.[15] Zobeidi et al.[16] used electrochemical methods and theoretical computation to examine the protection influence of azo Schiff base compounds against the corrosion of mild steel in 1.0 M HCl solution. The maximum inhibition efficiency for such compounds has been varied between 64.37 and 87.27% at 0.06 mM depending on the concentration and type of the azo Schiff base compound.

Received: April 1, 2024
Revised: May 17, 2024
Accepted: May 28, 2024
Published: June 21, 2024





https://doi.org/10.1021/acsomega.4c03135
*ACS Omega* 2024, 9, 29666−29681

The inhibition mechanism was attributed to the adsorption process, which results from the interaction between the N and O with the Fe on the steel's surface with a contribution of the $\pi$-electrons of the aromatic system to form an inhibitor film reducing the corrosion process.[16]

Our recent study focused on the synthesis of novel Schiff base compounds as inhibitors to resist the destruction of C-steel in hydrochloric acid media. $N^1$,$N^{1\prime}$-(ethane-1,2-dial)bis-($N^2$-(4-(dimethylamino)benzylidene))ethane-1,2-diamine (EDDB) and $N^1$-(4-(dimethylamino)benzylidene)-$N^2$-(2-((4-(dimethylamino)benzylidene)amino)ethyl)ethane-1,2-diamine (DBDB) are synthesized and confirmed as mitigators for the destruction of C-steel in 1.0 M HCl solution.[17,18] The inhibition efficacy reached 95.20% and 97.00% with EDDB and DBDB, respectively, at 5 mM and 298 K, confirming a mixed physical and chemical adsorption mechanism. In continuation with our work, an eco-friendly, cheap, and easy-to-prepare organic compound, namely, ($N^1E$)-$N^1$, $N^2$-bis(4-(dimethylamino) benzylidene)-ethane-1,2-diamine, DMAB, was synthesized to investigate the protection of the C-steel surface from the corrosive influence of $Cl^-$ ions preventing the metal damage. The DMAB compound is easily dissolved in the examined acidic media and does not affect the *p*H of the solution. Practical measurements were carried out to estimate the protection efficacy of such an inhibitor against the influence of the HCl solution. The mechanism of inhibition was investigated via an adsorption mechanism at various temperatures. The activation and adsorption thermodynamics parameters are evaluated and explained.

Quantum calculations performed by DFC have emanated as a helpful application for prognosticating the activity and stability of the organic substances in aqueous solutions.[19−21] Theoretical computations have been employed to elucidate the inhibition character of the DMAB compound by resolving some theoretical functions that rely on the type and nature of the adsorption of the utilized organic molecules onto the surface of the studied C-steel. The computation of theoretical data demonstrated by DFT was employed to establish the practical data of corrosion protection to discuss the distinctive adsorption of the DMAB organic inhibitor on the examined metal.

## 2. EXPERIMENTAL SECTION

**2.1. Electrodes and Chemicals.** The metallic coupons and the working electrode, WE, were made from C-steel, with little traces of a few other elements as depicted in Table 1.

**Table 1. Fourier-Transform Infrared Spectroscopy Analysis of C-Steel**

| element | Mn | C | Si | S | P | Fe |
|---|---|---|---|---|---|---|
| chemical composition, wt % | 0.60 | 0.20 | 0.39 | 0.03 | 0.03 | 99.35 |

Such materials were mechanically abraded utilizing suitable polishing papers with various grades. The execution for the metallic preparation and cleaning is similar to that depicted recently.[17] The organic chemicals 4-(dimethylamino)-benzaldehyde and ethane-1,2-diamine are Belgium chemicals with a purity of more than 99% without any further purification.

**2.2. Synthesis of DMAB Inhibitor.** The purpose of the synthesis of the ($N^1E$)-$N^1$,$N^2$-bis(4-(dimethylamino)-benzylidene)ethane-1,2-diamine compound, DMAB, is to examine the inhibition behavior for the destruction of the C-steel surface in dilute hydrochloric acid solution. 0.2 mol of 4-(dimethylamino)benzaldehyde was mixed with 0.1 mol of ethylenediamine into 0.250 L round-bottom flasks provided with a condenser in the presence of acetone. The reactants were refluxed by heating on a thermostatic water bath at 343 K for 4 h. The produced precipitate was evaporated from the solvent and washed completely utilizing acetone to remove the unreacted components. The product was evaporated from acetone followed by recrystallization, utilizing acetone to obtain a yield of about 99% (buff powder), ($N^1E$)-$N^1$, $N^2$-bis(4-(dimethylamino)benzylidene) ethane-1,2-diamine, Scheme 1.

The elemental analysis of the DMAB compound was proved by FTIR (Figure 1A) and mass spectroscopy (Figure 1B).

**2.3. Gravimetry Study.** The C-steel coupons have dimensions 74 mm × 22.9 mm × 2.9 mm. All samples are cut with the same dimensions and are polished with fine polishing papers, as indicated recently.[17] The polished C-steel samples were cleaned by washing under running tap water, then ultrasonically in distilled water, and finally dried before weighing using a digital electric balance, $W_1$. The weighted sample was immersed in 0.250 L of the examined solution for 8 h. The examined sample of C-steel was picked up from the solution, cleaned, and washed, followed by drying before reweighing again, $W_2$. Each test was achieved 3 times and the average value was considered. The data showed good reproducibility with a standard deviation ranging from 0.01 to 0.03. The examined solutions were dilute hydrochloric acid as a blank and inhibitive acid solutions containing various amounts of the DMAB compound. The tests were performed at various temperatures, 25−65 °C, utilizing an open-air thermostatic water bath supported by a temperature adjuster, ±0.1 °C.

The rate of the dissolution reaction ($r_g$) can be computed from the difference in the metallic sample weights, ($\Delta W = W_1 - W_2$), and the reaction time, *t*, and expressed in mg $cm^{-2}$ h utilizing the equation:[22,23]

$$r_g = \frac{\Delta W}{At} \tag{1}$$

where *A* is the total surface area of the investigated metal.

The coverage surface area ($\theta$) and the percentage of corrosion inhibition ($\eta_w$) of the DMAB compound were computed from the following relations:[10,23]

$$\theta = \left(1 - \frac{r_g}{r_c^\circ}\right) \tag{2}$$

$$\eta_w = \left(1 - \frac{r_g}{r_g^\circ}\right)100 \tag{3}$$

where $r_g^\circ$ and $r_g$ are the rate of corrosion in dilute acidic media, 1.0 M (blank), and the inhibitive acid solution containing the DMAB compound, respectively.

**2.4. Gasometry Study.** The same C-steel coupons were prepared as usual in the gravimetric study and utilized for the investigation of $H_2$ generation. The clean C-steel coupon was immersed in 0.250 L of the examined solution. After a short time of immersion, the $H_2$ started to release on the surface of the metal sample. The volume of the generated $H_2$ increased


https://doi.org/10.1021/acsomega.4c03135
ACS Omega 2024, 9, 29666−29681

**Scheme 1. Synthetic Scheme of the Newly Prepared DMAB Inhibitor**

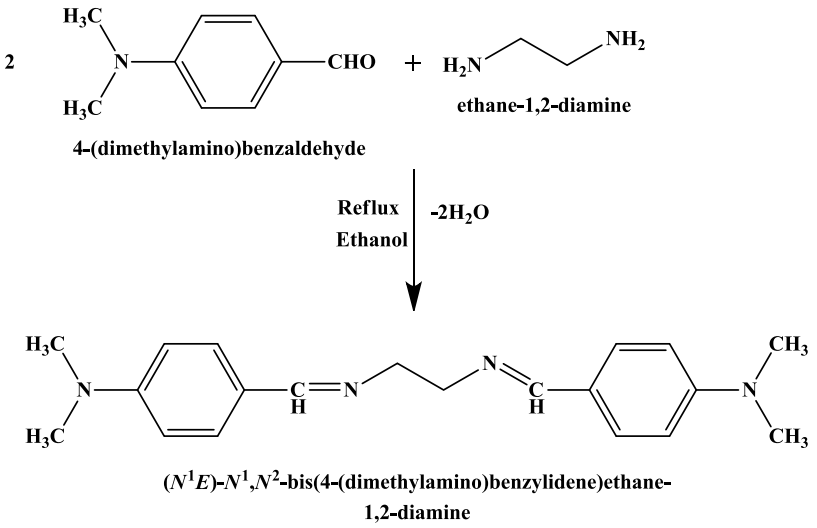


($N^1E$)-$N^1$,$N^2$-bis(4-(dimethylamino)benzylidene)ethane-1,2-diamine

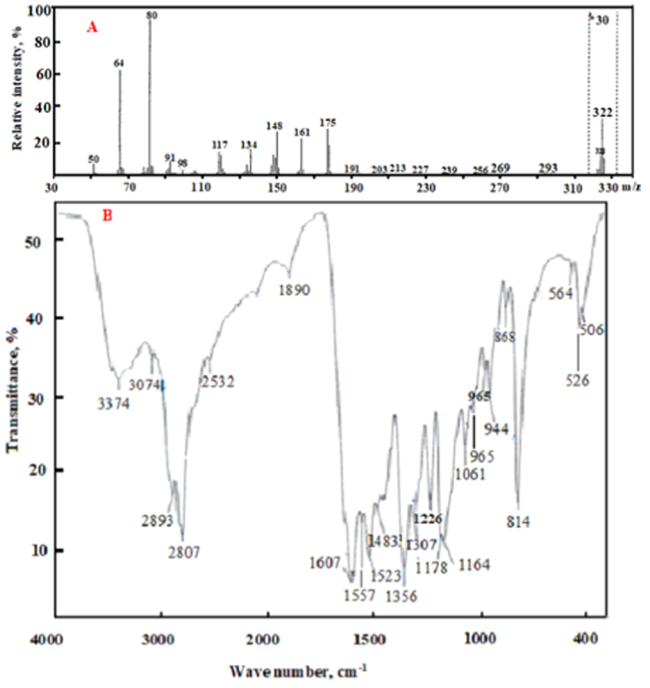


**Figure 1.** Mass spectrum (A) and infrared spectra (B) of the synthesized DMAB Schiff base compound.

with time and was collected over water in a graduated burette, as indicated earlier.[24] The reaction system used for generating $H_2$ was depicted early.[24,26]

The rate of the evolution of $H_2$, $r_H$, on the metallic surface was computed from the $V-t$ data. The covered surface area, $\theta$, and the percentage of corrosion inhibition, $\eta_H$, are computed from $r_H$ values, using eqs 4 and 5, respectively:[23]

$$\theta = \left(1 - \frac{r_H}{r_H^\circ}\right) \tag{4}$$

$$\eta_H = \left(1 - \frac{r_H}{r_H^\circ}\right) \tag{5}$$

where $r^\circ_H$ and $r_H$ are rates of the generated $H_2$ gas in the blank and the inhibitive DMAB solutions, respectively.

**2.5. Electrochemical Study.** A potentiostat (potentiostat PGZ 301-model) was utilized for the potentiodynamic polarization (PD) and EIS investigations.[17] A double-wall cell provided by a 3-electrode configuration was utilized. A C-steel was utilized as a working electrode, WE, where its potential, $E$, was measured relative to a saturated calomel reference electrode, SCE. A Pt plate with a surface area of ~2.0 $cm^2$ was utilized as an auxiliary electrode. The WE was prepared as a suitable cylindrical rod of C-steel and inserted into a glass tube, leaving a free bottom area of 0.38 $cm^2$ to be in contact with the examined solution during measurements. The WE was polished with various grades of fine emery papers starting with rough ones. Then, the WE was washed several times with distilled water and acetone, directly before carrying the measurement. The WE was first immersed in the investigated solution till the $E_{st}$ value was attained. Each run was duplicated to estimate reproducibility and average values of the electrochemical parameters were reported. The $E$-log $I$ plots were organized when the potential of the WE was allowed to change from −0.85 to −0.35 V to the SCE at $E_{corr}$ with a scan rate of 0.2 mV $s^{-1}$ at 298 K.

The surface coverage $\theta$ and the protection efficacy ($\eta_p$) were computed from the values of the corrosion current densities, according to the relations:[26−28]

$$\theta = \left(1 - \frac{I_{corr}}{I_{corr}^\circ}\right) \tag{6}$$

$$\eta_p = \left(1 - \frac{I_{corr}}{I_{corr}^\circ}\right)100 \tag{7}$$

where $I_{corr}^\circ$ and $I_{corr}$ are the corrosion current densities in 1.0 M HCl solution free of and mixed with the DMAB inhibitor.

The EIS measurements were performed when the frequency was allowed to vary between 100 kHz and 0.005 Hz at an open-circuit potential, utilizing an A.C. of 10 mV via the working cell. The gained EIS data were fitted using the ZSimpWin approach.[19] The charge transfer resistances, $R_{ct}^\circ$ for the blank electrolyte and $R_{ct}$ in the presence of the DMAB compound, were utilized to determine the values of the surface



https://doi.org/10.1021/acsomega.4c03135
ACS Omega 2024, 9, 29666−29681

coverage, $\theta$, and the protection efficacy ($\eta_I$) using eqs 8 and 9, respectively:[28,29]

$$\theta = \left(1 - \frac{R_{ct}^{\circ}}{R_{ct}}\right) \tag{8}$$

$$\eta_{I=}\left(1 - \frac{R_{ct}^{\circ}}{R_{ct}}\right)100 \tag{9}$$

Utilizing $\omega_{max} = 2\pi f_{max}$, the double-layer capacitance, $C_{dl}$, can be computed utilizing the relation:[30,31]

$$C_{dl} = Y_{o}(\omega_{max})^{n-1} \tag{10}$$

**2.6. Surface Analysis.** To explain the change in the morphology of the surface appearance for the clean dry C-steel electrodes before and after the corrosion and inhibition processes, three specimens of C-steel were employed. One sample was immersed in 1.0 M HCl solution, and the other was introduced in the same acid concentration containing 5.0 mM of the DMAB compound at 298 K. After a period of 4 h, the examined specimens were picked up from the different electrolytes, washed using distilled water, and dried in a desiccator. The morphology of the examined C-steel surface was investigated under scanning electron microscopy, SEM, of a type A Jeol, JSM-5410 (Japan).

**2.7. Quantum Computations.** The best geometries for the DMAB inhibitor molecules were computed by DFT using the B3LYP and 6−31g (d,p). The calculations were performed in the aqueous phase as explained in the recent literature,[32] where quantum chemical factors were gained with the G09 code.[33] Various factors, such as $\Delta E$, $\eta$, $\sigma$, and the transferred $e^-$, $\Delta N$, were computed utilizing eqs 11−14, respectively:[17]

$$\text{energy gap, } \Delta E = E_{LUMO} - E_{HOMO} \tag{11}$$

$$\text{hardness, } \eta = \frac{\Delta E}{2} \tag{12}$$

$$\text{softness, } \sigma = \frac{1}{\eta} \tag{13}$$

$$\Delta N_{110} = \frac{\varphi - x_{inh}}{2(\eta_{Fe} + \eta_{inh})} \tag{14}$$

where $x_{inh}$ and $\eta_{inh}$ resemble the electronegativity and the hardness of the DMAB inhibitor, respectively, while $\eta_{Fe}$ and $\varphi$ are the hardness of iron and the work function, respectively.

MC simulation was performed to inspect the kind of interaction between the DMAB and the iron.[17] The iron surface was prepared by cleaving with (110) as the most stable surface to simulate the adsorption process. The Fe(110) was enlarged to a supercell (15 × 15) with a vacuum 30 Å thickness built on the Fe plane (110). The COMPASS force field and Ewald summation technique were used. The needed adsorption energy, $E_{ads}$, between the DMAB compound and the metal surface was computed by the relation:

$$E_{ads} = E_{Fe\text{-}inh} - E_{inh} - E_{Fe} \tag{15}$$

where $E_{Fe\text{-}inh}$, $E_{inh}$, and $E_{Fe}$ are the energies of the DMAB molecules over the metal, the DMAB molecule, and the iron on the surface of the steel, respectively.

## 3. RESULTS AND DISCUSSION

**3.1. Structure of DMAB Confirmation.** The data of FTIR and mass spectroscopy were utilized to confirm the chemical structure of the ($N^1E$)-$N^1$,$N^2$-bis(4-(dimethylamino)-benzylidene)ethane-1,2-diamine compound, DMAB.

*3.1.1. FTIR Study.* The measured infrared spectra of the DMAB compound are summarized in Table 2, as depicted in Figure 1A. The results explain the existence of CH aromatic stretching at 3074 $cm^{-1}$, CH aliphatic symmetric stretching at 2893 $cm^{-1}$, CH aliphatic asymmetric stretching at 2807 $cm^{-1}$, C=N stretching at 1605 $cm^{-1}$, C=C aromatic stretching at 1557 $cm^{-1}$, $CH_2$ bending 1483 $cm^{-1}$, $CH_3$ bending at 1356 $cm^{-1}$, C−N aryl stretching at 1307 $cm^{-1}$, C−N alkyl stretching at 1178 $cm^{-1}$, CH para bending at 814 $cm^{-1}$, and CH ortho bending at 723 $cm^{-1}$.

**Table 2. Fourier-Transform Infrared Spectroscopy Analysis of the DMAB Compound**

| band | $\nu$, 1/cm |
|---|---|
| C−H aromatic stretching | 3074 |
| C−H aliphatic symmetric stretching | 2893 |
| C−H aliphatic asymmetric stretching | 2807 |
| CN stretching | 1605 |
| CC aromatic stretching | 1557 |
| $CH_2$ bending | 1483 |
| $CH_3$ bending | 1356 |
| CN aryl stretching | 1307 |
| CN alkyl stretching | 1178 |
| CH para bending | 814 |
| CH ortho bending | 723 |

*3.1.2. Mass Spectroscopy, MS, Study.* Figure 1B shows the mass spectra of the synthesized DMAB molecule. The measurements of the proposed chemical formula of the DMAB substance show a peak at $m/z$ 322 (1.18%), which is related to the molecular ion (parent peak). The group of peaks at 161 (21.77% [$(CH_3)_2$-N-$C_6H_4$-CH=N-$CH_2$)] served as a base peak jointly with other ones observed at 80 (100% (C=N-$CH_2$-$CH_2$-N=C), 134 (15.72% [$(CH_3)_2$-N-$C_6H_4$-$CH_2$]), and 148 (26.01% [$(CH_3)_2$-N-$C_6H_4$-CH=NH)]).

**3.2. Gravimetry Measurements.** The gravimetry study was done to investigate the destruction attitude of dilute HCl solution and the retardation effect of the DMAB substance toward the C-steel at various temperatures. Table 3 depicts the values of corrosion rate ($r_g$), surface coverage ($\theta$), and inhibition efficacy ($\eta_w$). The $r_g$ value is lowered by raising the DMAB amount in the aqueous acidic solution and increased with temperature. Figure 2A represents the reduction in the corrosion rate, $r_g$, by increasing the DMAB concentration at different temperatures. Increasing the amount of the DMAB inhibitor in the aggressive media diminishes the $r_g$ and increases the protection efficacy ($\eta_w$), as shown in Table 3 and Figure 2B. The sigmoidal plots of Figure 2B confirm the adsorbability character of the DMAB compound against the destruction of the metal surface by the effect of chloride ions in the aqueous solution.[30,45] The reduction in the $\theta$ and the $\eta_w$ values for the DMAB inhibitor with temperature could explain the leaving of some of the already adsorbed DMAB molecules from the metal surface into the bulk of the solution as the temperature increased. This attitude is owing to the nature of the adsorption process between the DMAB molecules and the


https://doi.org/10.1021/acsomega.4c03135
ACS Omega 2024, 9, 29666−29681

Table 3. Values of Rate of Corrosion, $r_g$, mg cm$^{-2}$ h$^{-1}$, Surface Coverage, $\theta$, and the Anticorrosion Efficiency, $\eta_w$, for C-Steel in 1.0 M HCl without and with the DMAB Compound at Various Temperatures (Gravimetric Data)

| | 298 K | | | 313 K | | | 338 K | | |
|---|---|---|---|---|---|---|---|---|---|
| conc., mM | $r_g$, mg cm$^{-2}$ h$^{-1}$ | $\theta$ | $\eta_w$ (%) | $r_g$, mg cm$^{-2}$ h$^{-1}$ | $\theta$ | $\eta_w$ (%) | $r_g$, mg cm$^{-2}$ h$^{-1}$ | $\theta$ | $\eta_w$ (%) |
| 0.00 | 1.0494 | | | 2.0051 | | | 3.3874 | | |
| 0.05 | 0.2962 | 0.72 | 71.77 | 0.7843 | 0.61 | 60.89 | 1.5928 | 0.53 | 52.98 |
| 0.10 | 0.2596 | 0.75 | 75.26 | 0.6652 | 0.67 | 66.83 | 1.4459 | 0.57 | 57.32 |
| 0.50 | 0.2179 | 0.79 | 79.24 | 0.5635 | 0.72 | 71.90 | 1.2066 | 0.64 | 64.38 |
| 1.00 | 0.1570 | 0.85 | 85.03 | 0.4473 | 0.78 | 77.69 | 1.0098 | 0.70 | 70.19 |
| 5.00 | 0.0838 | 0.92 | 92.01 | 0.3298 | 0.84 | 83.55 | 0.8526 | 0.75 | 74.83 |

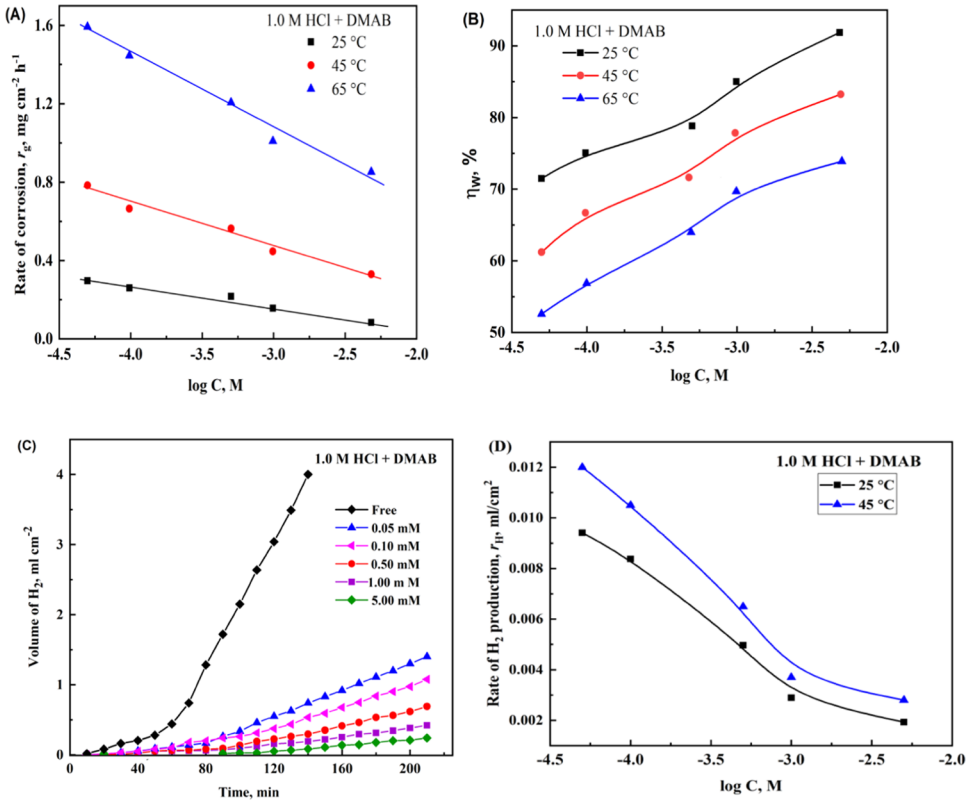


Figure 2. Variation of the rate of corrosion $r_g$ (A) and $\eta_w$% with log C of the DMAB compound (B), volume−time curves (C), and variation of $r_{H_2}$ with log C of DMAB (D) for C-steel in 1.0 M HCl.

metal surface, which depends on the electrostatic attraction, i.e., physisorption.[37]

**3.3. Gasometric Measurements.** The protection behavior of the DMAB compound against the corrosion of C-steel and the $H_2$ production was investigated by the gasometric method. In this study, the volume of the generated $H_2$ ($V_H$) is increased as the immersion time ($t$) is elongated, which depends on the DMAB amount and the solution temperature. The constructed $V_H$−$t$ plots when the C-steel metal is immersed in a dilute hydrochloric acid electrolyte without the DMAB inhibitor and in the existence of different additions of DMAB are shown in Figure 2C. The decrease in the $r_H$ values with more amounts of the DMAB compound, Figure 2D, is due to the reduction in the generated hydrogen, $V_H$ on the metallic sample, due to the inhibition effect.

The generated hydrogen accumulates on the corroded metal surface after a certain interval, incubation time, $\tau$, at which the oxide layer starts to be broken by $Cl^-$ ions in the investigated solution.[23,35,36] After the incubation time, $V_H$ gradually increases with the immersion time due to the continuous dissolution of the bare metal surface.[23] The $\tau$ is elongated as the added amount of the DMAB compound is raised and is decreased with temperature, confirming the inhibition of metal destruction. Such an attitude would explain the inhibition influence by the added DMAB compound via the adsorption of such inhibitor molecules on the investigated metal sample. The variation in the rate of the produced $H_2$, $r_H$ with the amount of the DMAB compound, at 298 and 318 K, is depicted in Figure 2D and Table 4. The data $r_H$-log $C_{inh}$ explains S-shaped plots similar to that obtained by the gravimetric method, proving the adsorption of the DMAB molecules on the investigated steel surface.[35]

The values of $\theta$ and $\eta_H$ % computed with various amounts of the DMAB substance are shown in Table 4, which are increased with increasing the added DMAB inhibitor and are reduced with increasing the temperature. The reduction in the $\theta$ and $\eta_H$ % values with increasing temperature could be related to the reduction in the $r_H$ values, which proves the desorption of a few of the already adsorbed DMAB molecules escaping into the bulk of the solution. Such an attitude could explain the


https://doi.org/10.1021/acsomega.4c03135
ACS Omega 2024, 9, 29666−29681

**Table 4. Values of $r_g$, mL/cm$^2$, $\theta$, and $\eta_H$ for C-Steel in 1.0 M HCl without and with the DMAB Compound, at Various Temperatures, at 298 and 318 K (Gasometry Data)**

| conc., mM | $r_H$, mL cm$^{-2}$ | $\theta$ | $\eta_H$ |
|---|---|---|---|
| 0.00 | 0.04759 [0.0871][a] | | |
| 0.05 | 0.01152 [0.0245] | 0.764 [0.719] | 76.4 [71.9] |
| 0.10 | 0.00927 [0.0195] | 0.805 [0.776] | 80.5 [77.6] |
| 0.50 | 0.00805 [0.0172] | 0.830 [0.803] | 83.1 [80.3] |
| 1.00 | 0.00492 [0.0135] | 0.897 [0.845] | 89.7 [84.5] |
| 5.00 | 0.00292 [0.0075] | 0.939[0.913] | 93.3 [91.3] |

[a]The second value was obtained at 318 K.

possibility of the DMAB molecules being electrostatically adsorbed on the corroded metal surface.[34]

**3.4. Potentiodynamic Polarization, PD, Study.** The PD plots of the investigated C-steel in the HCl solution free of and mixed with the DMAB compound are depicted in Figure 3.

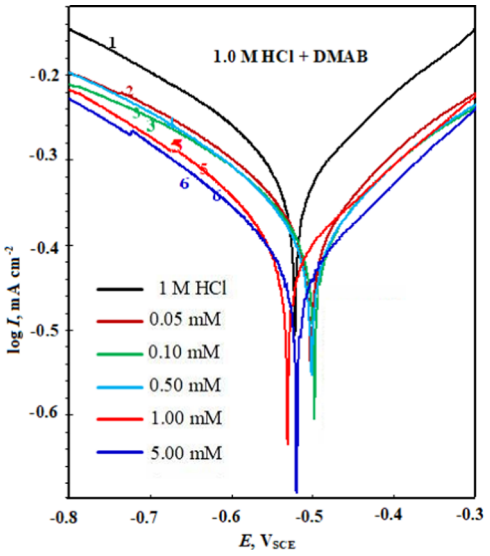


**Figure 3.** Potentiodynamic polarization curves of C-steel in 1.0 M HCl solution devoid of and containing different additions of the DMAB compound.

Different corrosion parameters, i.e., $E_{corr}$, $I_{corr}$, $\beta_a$, $\beta_c$, $R_p$, and $\eta_p$, were computed and listed in Table 5. It is noticed that the values of the corrosion current, $I_{corr}$, are reduced with more additions of the DMAB compound due to an inhibition effect. Also, the values of the anodic and cathodic Tafel slopes $\beta_a$ and $\beta_c$ do not display a marked change that is attributed to the similarity in the corrosion mechanism in the absence and existence of the DMAB molecules. Such an attitude explains that the DMAB compound decreases the anodic and cathodic half-reactions.[37,38]

**Table 5. Potentiodynamic Polarization Constants Computed for C-Steel in 1.0 M HCl Free of and Mixed with Various Additions of the DMAB Compound at 298 K**

| conc., mM | $E_{corr}$, mV, SCE | $I_{corr}$, mA cm$^{-2}$ | $B_a$, mV dec$^{-1}$ | $B_c$, mV dec$^{-1}$ | $R_p$ | $\eta_p$, % |
|---|---|---|---|---|---|---|
| 0.00 | −524 | 1.0697 | 153 | −179 | 42 | |
| 0.05 | −504 | 0.3117 | 155 | −174 | 158 | 73.41 |
| 0.10 | −500 | 0.2691 | 166 | −189 | 191 | 78.01 |
| 0.50 | −503 | 0.2387 | 158 | −167 | 204 | 79.41 |
| 1.00 | −533 | 0.1750 | 162 | −166 | 283 | 85.16 |
| 5.00 | −522 | 0.0915 | 138 | −148 | 450 | 90.37 |

In addition, Figure 3 shows that the added DMAB does not have a serious effect on the values of $E_{corr}$ concerning that of the blank solution. Such an attitude confirms that the DMAB compound resists the anodic iron dissolution and $H_2$ production reactions. The change in the $\Delta E_{corr}$ values between the blank solution and that of the DMAB inhibitor solution varies within 24 mV, proving that the DMAB substance acts as a mixed-type inhibitor.[37,39]

The protection efficacy, $\eta_p$, of the DMAB compound was computed from the $I_{corr}$ values for the blank solution and the DMAB inhibitive solution utilizing eq 6. The protection efficacy, $\eta_p$, is found to take higher values with higher amounts of the DMAB compound due to the decrease in the $I_{corr}$ values. This could explain the inhibition of the anodic and cathodic half-reactions by the DMAB molecules that block the reactive centers on the surface of the investigated metal.[17]

Moreover, the existence of the DMAB compound increases the value of $R_p$ from 42 Ω cm$^2$ (in the free acid solution) to 450 Ω cm$^2$ at a concentration of 5.0 mM DMAB compound that proves the consistency of the formed film on the metallic surface owing to an adsorption phenomenon. The increase in the values of $R_p$ and $\eta_p$ with higher amounts of the DMAB substance could explain the growth of the adsorbed DMAB molecule layer on the surface of the investigated metal.[17]

**3.5. Measurements of Impedance, EIS, Study.** The EIS measurements are utilized as a nondestructive tool to investigate the Nyquist plots of the examined metal in dilute HCl media devoid of and containing the DMAB inhibitor at different additions (Figure 4). The EIS spectra of the

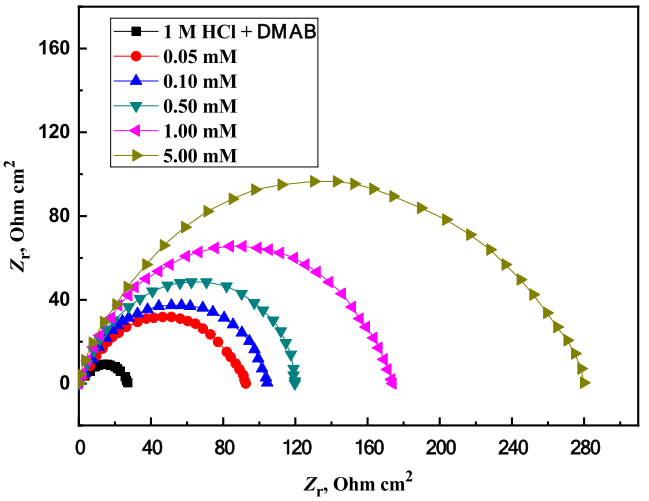


**Figure 4.** Nyquist plots of C-steel in 1.0 M HCl solution without and with different additions of the DMAB Schiff base compound at 25 °C.

investigated metal have been extremely adjusted when the DMAB molecule is mixed with the aggressive acidic media. The Nyquist curves can be demonstrated via the equivalent circuit depicted in Figure 5, which has been used already for the Fe/H$^+$ interface.[40]

Figure 4 indicates a depressed semicircle capacitive loop that appears with the existence of the DMAB molecules mixed with the destructive hydrochloric acid media, not typical semicircles as expected from the impedance view. The presence of such


https://doi.org/10.1021/acsomega.4c03135
ACS Omega 2024, 9, 29666−29681

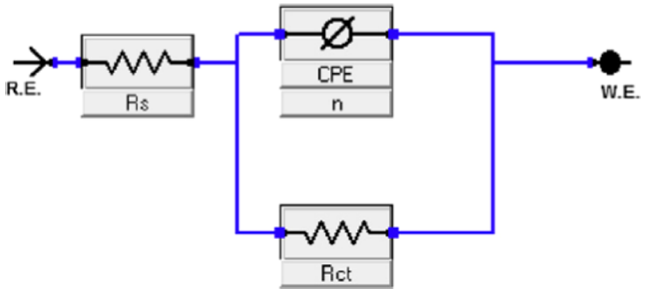


**Figure 5.** Equivalent circuit model was used to fit the EIS data in the absence and presence of the DMAB Schiff base compound.

capacitive loops in the full investigated frequency range for the acid-aggressive and the inhibitive media confirms that the protection process for the corroded metal surface against the corrosive action of the HCl solution is accompanied by the charge transfer process between the metallic surface and the DMAB substance.[41,42] The DMAB compound behaves as an interface inhibitor that adsorbs at the C-steel/$H^+$ interface forming an inhibitor adsorbed layer that lowers the corrosive effect of hydrochloric acid.[43] Increasing the added amount of the DMAB substance into the HCl media gradually reduces the diameter of the capacitive loop, explaining the growth of the inhibitive adsorbed layer on the surface of the examined metal that lowers the contact between the metallic surface and the HCl solution.

The Bode ($\log f$ against log imaginary impedance) and the phase angle curves ($\log f$ against log phase angle) are utilized to investigate the inhibitive influence of DMAB toward the destruction of the metal surface in dilute hydrochloric media as depicted in Figure 6. Bode plots indicate a capacitive zone at

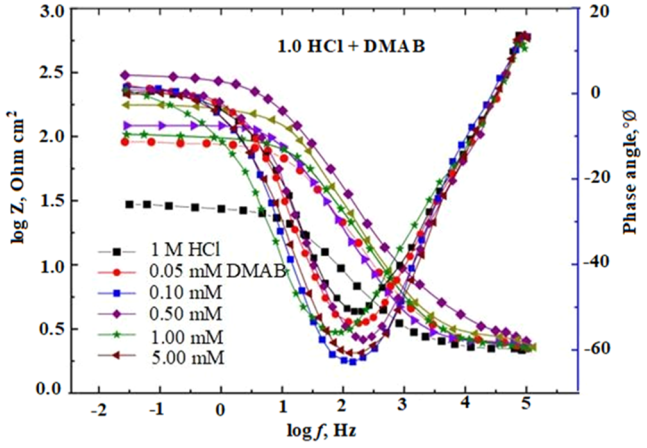


**Figure 6.** Bode and phase angle plots of C-steel in 1 M HCl solutions without and with various concentrations of the DMAB Schiff base compound.

intermediate frequencies and a resistive region at high and low frequencies. The increase in the height of peaks of Bode phase plots with more additions of the DMAB compound could be attributed to the formation of a protective film on the C-steel surface.[44,45] Such behavior increases the inhibition efficacy, $\eta_I$, with more additions of the inhibitor.[16] Also, in Figure 6, the phase angle is shifted into the more negative values with more additions of the DMAB compound, explaining the existence of an adsorbed film of the DMAB compound that protects the steel surface from being in contact with $Cl^-$ ions.[16,46,47]

Different corrosion parameters obtained by impedance measurements, such as $R_{ct}$, $C_{dl}$, and the protection efficacy, $\eta_I$, are determined by analyzing the gained data of the impedance measurements, which are shown in Table 6. The rise in the $R_{ct}$ values with more amounts of the DMAB substance in the hydrochloric acid media (1.0 M) could confirm the rise in the capability of the DMAB substance to be adsorbed on the surface of the investigated steel, lowering the rate of the corrosion reaction.[16] Also, the values of the double-layer capacitance, $C_{dl}$, decreased as the amount of the DMAB molecules increased, which could confirm the greater thickness of the electrical double layer due to the reduction in the rate of metal corrosion, emphasizing the adsorption of the DMAB substance on the investigated metal.[16,48]

**3.6. Comparison of the Inhibition Efficacy with Other Schiff Base Compounds.** The inhibition efficacy of the DMAB Schiff base compound as an acidic inhibitor was compared to that of other Schiff base derivatives in various acidic solutions.[13−19] The computed $\eta$ % has been determined and matched with comparable types of the Schiff base molecules,[13−19,24,49,50] as depicted in Table 7. The results reveal that the examined DMAB is projected to work similarly to, if not better than, other previously examined Schiff base compounds when utilized at significantly lower amounts.

**3.7. Mechanism of Adsorption.** The protection of metallic surfaces from the corrosion process by adding organic molecules into the corrosion environment is controlled by the adsorption of the inhibitive organic compounds on the invested metallic surface. The adsorption process is found to be dependent on some variables, including the number of adsorption sites located on the inhibiting molecule as well as the temperature of the solution. The adsorption process involves a substitution step between the used inhibitive organic molecules and the $H_2O$ molecules adsorbed on the metallic surface. Such a process is considered a quasi-exchange process that can be summarized by the relation:[51]

$$DMAB_{(sol)} + zW_{(ads)} \leftrightarrow DMAB_{(ads)} + zW_{(sol)} \quad (16)$$

where $z$ resembles the number of desorbed water molecules, $W_{(ads)}$, substituted by only a $DMAB_{(ads)}$ molecule.

Temkin, Freundlich, Frumkin, and Langmuir's adsorption isotherms were used to investigate the adsorption of the

**Table 6. EIS Data of C-Steel in 1.0 M HCl Free of and Mixed with Various Additions of the DMAB Compound at 298 K**

| conc., M | $R_s$, Ω cm$^2$ | $Q_{dl}$, $10^4$, Ω$^{-1}$ s$^n$ cm$^{-2}$ | $n$ | error of $n$ | $R_{ct}$, Ω cm$^2$ | $C_{dl}$, μF cm$^{-2}$ | $\eta_I$ % |
|---|---|---|---|---|---|---|---|
| 0.00 | 839.7 | 0.2215 | 0.83 | 1.22 | 25.4 | 280.4 | |
| $5 \times 10^{-5}$ | 2.40 | 0.513 | 0.85 | 1.04 | 89.10 | 89.3 | 71.5 |
| $1 \times 10^{-4}$ | 2.60 | 0.437 | 0.64 | 1.12 | 102.0 | 70.0 | 75.1 |
| $5 \times 10^{-4}$ | 2.30 | 0.359 | 0.80 | 0.83 | 118.0 | 108 | 78.5 |
| $1 \times 10^{-3}$ | 2.70 | 0.246 | 0.70 | 0.50 | 169.0 | 75.0 | 85.0 |
| $5 \times 10^{-3}$ | 4.60 | 0.110 | 0.70 | 0.50 | 290.0 | 73.0 | 91.2 |



https://doi.org/10.1021/acsomega.4c03135
ACS Omega 2024, 9, 29666−29681

**Table 7. Comparison of $\eta$ % Values of DMAB with Other Similar Compounds**

| Schiff base compound and the corrosive solution | conc$^n$. | $\eta$% | ref. |
|---|---|---|---|
| 2,2′-(heptane-1,7-diylbis(azanylylidene)bis-(methanylylidene))diphenol, 0.5 M $H_2SO_4$ | 1 mM | 93.6 | 2 |
| 3-((5-mercapto-1,3,4-thiadiazol-2-yl) imino)indolin-2-one, 1.0 M HCl | 0.5 mM | 96.4 | 15 |
| *N*-(2-((*Z*)-2-(benzylideneamino)ethylamino)- ethyl)3,4,5-trihydroxybenzamide, 0.5 M HCl | 250 ppm | 88.6 | 16 |
| $N^1$,$N^{1'}$-(ethane-1,2-diyl)bis(N2-(4-(dimethylamino) benzylidene)ethane-1,2-diamine), 1.0 M HCl | 5 mM | 95.2 | 17 |
| 2,4-bis-(2- hydroxynaphthaldehyde)diiminotholuene, 1.0 M HCl | 5 mM | 85.6 | 19 |
| *N*1-(4-(dimethylamino)benzylidene)-$N^2$-(2-((4-(di- methylamino)benzylidene)amino)ethyl)ethane-1,2-diamine, 1.0 M HCl | 5 mM | 97.0 | 24 |
| 4-((*E*)-(3-((*E*)-(Hexylimino)methyl)-4-hydroxyphenyl)diazenyl)benzonitrile, 1.0 M HCl | 100 ppm | 90.1 | 49 |
| 4-((*E*)-(3-((*E*)-(Dodecylimino)methyl)-4-hydroxyphenyl)- diazenyl)benzonitrile, 1.0 M HCl | 100 ppm | 92.4 | 49 |
| 4-amino-*N*-benzylidene-benzamide, 1.0 M HCl | 10 mM | 96.0 | 50 |
| ($N^1E$)-$N^1$,$N^2$-bis(4-(dimethylamino)benzylidene)ethane-1,2-diamine | 5.0 mM | 97.7 | present study |

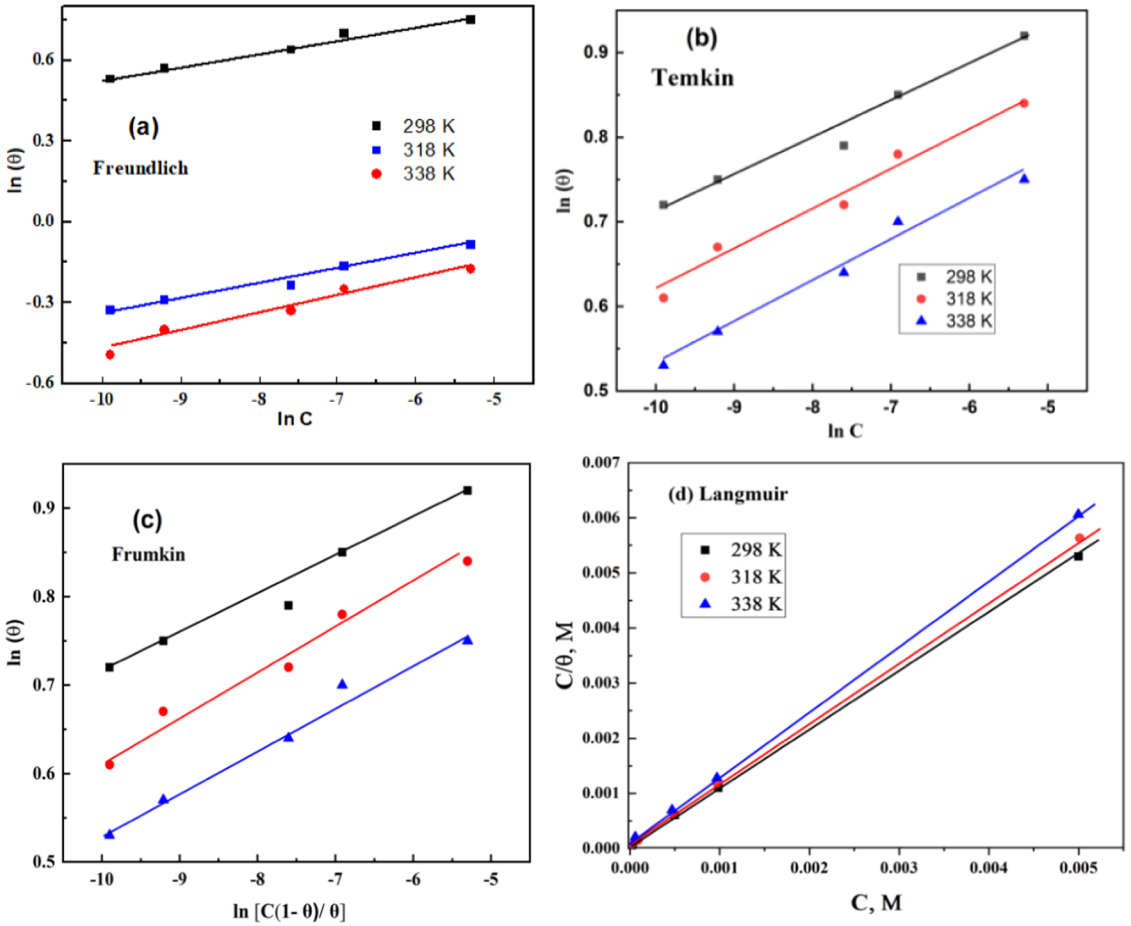


**Figure 7.** Adsorption isotherms of the DMAB Schiff base compound on the C-steel surface in 1.0 M HCl at various temperatures.

utilized DMAB compound on the carbon steel surface in the oilfield-produced water. The adsorption isotherm models are given by the following equations:[52,53]

$$\text{Temkin } K_{ads}C = e^{f\theta} \tag{17}$$

$$\text{Frundlich } \theta = K_{ads}C^n \tag{18}$$

$$\text{Frumkin } \frac{\theta}{1-\theta}e^{-2f\theta} = K_{ads}C \tag{19}$$

$$\text{Langmuir } \frac{C}{\theta} = \frac{1}{K_{ads}} + C \tag{20}$$

The experimental data obtained from gravimetry are utilized to fit the best suitable adsorption isotherm. The best-fitted isotherm was Langmuir with a regression coefficient, $R^2$, as well as the slopes close to unity, confirming that the Langmuir model is the suitable adsorption isotherm for the DMAB compound on the C-steel surface, which is illustrated by the formation of a single adsorbed layer.[24,25]

According to the Langmuir equation represented by eq 20, C resembles the equilibrium concentration of the DMAB compound in mol $L^{-1}$, $\theta$ represents the surface coverage induced by the DMAB molecules, and $K_{ads}$ is the equilibrium constant of the adsorption−desorption process. The data of Figure 7 affirms the plotting of $C\theta^{-1}$ against the DMAB concentration, *C*. The figure shows straight lines with strong positive correlation coefficients ($r \sim 1$) with slopes equal to 1, which proves that adsorption is controlled by Langmuir's model. The $K_{ads}$ value can be computed from the intercept


https://doi.org/10.1021/acsomega.4c03135
ACS Omega 2024, 9, 29666−29681

Table 8. Values of the Equilibrium Constants, $K_{ads}$, Free Energy, $\Delta G^{\circ}_{ads}$, Enthalpy, $\Delta H^{\circ}_{ads}$, and Entropy, $\Delta S^{\circ}_{ads}$, of the Adsorption of the DMAB Compound on C-Steel in 1.0 M Hydrochloric Acid at Various Temperatures

| $T$, °C | $K_{ads} \times 10^4$, $M^{-1}$ | $\Delta G^{\circ}_{ads}$, kJ $mol^{-1}$ | $\Delta H^{\circ}_{ads}$, kJ $mol^{-1}$ | $\Delta S^{\circ}_{ads}$, J $mol^{-1}$ $K^{-1}$ |
|---|---|---|---|---|
| 298 | 2.59 | −35.13 | | 89.32 |
| 308 | 2.05 | −36.87 | −8.51 | 89.17 |
| 318 | 1.72 | −38.70 | | 89.32 |

point with the $Y$-axis of Figure 7, $K_{ads}$ = 1/intercept. The $K_{ads}$ values listed in Table 8 are reduced with the rise in temperature, explaining the desorption of some molecules of already adsorbed DMAB molecules leaving the steel surface escaping into the bulk of the solution, as the temperature increased. The computed $K_{ads}$ values, Table 8, are used to determine the thermodynamic function $\Delta G^{\circ}_{ads}$, which is known as the standard free energy of adsorption utilizing the relation:[54]

$$\Delta G^{\circ}_{ads} = -RT[\ln K_{ads} + 4.0164] \quad (21)$$

where 4.016 is a constant that corresponds to the logarithmic concentration of $H_2O$. The values $\Delta G^{\circ}_{ads}$ are depicted in Table 8 and vary between −35.13 and −38.70 kJ $mol^{-1}$. These data are characterized by the minus sign that could confirm the spontaneity of the adsorption of DMAB molecules on the investigated C-steel surface.[55,56] The value $\Delta G^{\circ}_{ads}$ is less than 20 kJ $mol^{-1}$ and higher to reach 40 kJ $mol^{-1}$, emphasizing the physical- and chemisorption mechanism of the DMAB molecules on the corroded C-steel.[55] The reduction in the values of $\Delta G^{\circ}_{ads}$ with temperature would illustrate that the inhibition process by the DMAB inhibitor molecules is endothermic.[39,56]

In addition, the computed $K_{ads}$ values are useful to determine the thermodynamic function standard enthalpy, $\Delta H^{\circ}_{ads}$, for the adsorption process via the relation:[54]

$$\ln K_{ads} = \left(\frac{-\Delta H^{\circ}_{ads}}{RT}\right) + \text{constant} \quad (22)$$

Such a relation can be represented in Figure 8, ln $K_{ads}$ values versus $T^{-1}$, which produces straight line plots of a slope equal to $-\Delta H^{\circ}_{ads}/R$. The deduced $\Delta H^{\circ}_{ads}$ values shown in Table 8 indicate the negative sign, which proves that the adsorption of DMAB inhibitor molecules on the corroded steel surface is an exothermic process.[57] Such a conclusion could explain the decrease in the protection efficacy with the temperature, which confirms the desorption of a few numbers of already adsorbed DMAB inhibitor molecules from the corroded metal surface into the bulk of the solution, as the temperature increased. On the other hand, a chemisorption process is approved when the $\Delta H^{\circ}_{ads}$ take values more than 40 kJ $mol^{-1}$ and can reach 400 kJ $mol^{-1}$. The computed $\Delta H^{\circ}_{ads}$ is equal to −8.51 kJ $mol^{-1}$, which sustains the electrostatic adsorption of the DMAB molecules on the corroded steel.

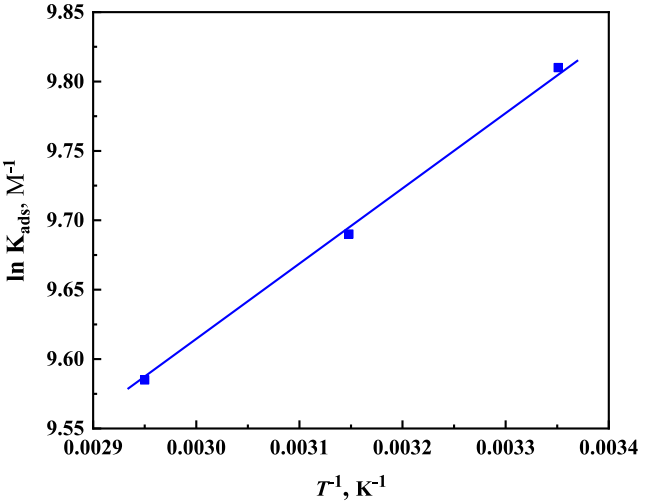


Figure 8. Van't Hoff plots (ln $k$ versus $1/T$) for the corrosion of C-steel in 1.0 M HCl.

Also, the thermodynamic function standard entropy, $\Delta S^{\circ}_{ads}$, values can be computed from the relation:[54]

$$\Delta G^{\circ}_{ads} = \Delta H^{\circ}_{ads} - T\Delta S^{\circ}_{ads} \quad (23)$$

The obtained $\Delta S^{\circ}_{ads}$ values take a positive sign and almost have the same value, Table 8, which illustrates that the adsorption of DMAB inhibitor molecules is associated with a small variation in entropy value.

**3.8. Adsorption Modes for DMAB.** The large values of $K_{ads}$ indicate the strong adsorption of DMAB on C-steel. This agrees with the higher values of the inhibition efficacy obtained from different methods reaching 97%. The value of free energy, $\Delta G^{\circ}_{ads}$, tends to be −40 kJ $mol^{-1}$, also, the enthalpy, $\Delta H^{\circ}_{ads}$, has a negative value and near to be zero. This confirms that the adsorption of DMAB on the C-steel surface tends to be more chemisorption than physisorption. The inhibition of DMAB on C-steel in 1.0 M hydrochloric acid can occur through the adsorption of lone pairs of electrons of two nitrogen atoms and double bonds of two benzene rings on cathodic sites of the C-steel surface as shown in Figure 9.

**3.9. Influence of Temperature.** Arrhenius equation is used to compute the activation energy ($E_a$) accompanied by the dissolution process and investigate the mechanism of corrosion protection of C-steel in 1.0 M HCl solutions. The values of $r_g$ computed by gravimetric measurements in the absence and presence of the DMAB inhibitor at various temperatures are used. The $r_g$ values are varied with temperature, $T$, according to the relation:[54]

$$\log r_g = \left(\frac{-E_a}{2.303R}\right) + \text{constant} \quad (24)$$

where $E_a$ represents the energy of activation of the dissolution reaction and $R$ is the Arrhenius constant. Figure 10 represents the variation of the log $r_g$ values versus $T^{-1}$ for all the investigated dilute HCl free of and mixed with various amounts of the DMAB compound. Such plots produce straight line relations with strong positive correlation coefficients very close to one, which confirms applications of the Arrhenius relation. The $E_a$ values are deduced from the slope of the constructed line plots that are listed in Table 9. The higher values of $E_a$ computed in the existence of the DMAB compound with a decrease in the protection efficacy would offer the probability of the physisorption process of the DMAB compound on the examined metal surface.[58−61]



https://doi.org/10.1021/acsomega.4c03135
ACS Omega 2024, 9, 29666−29681

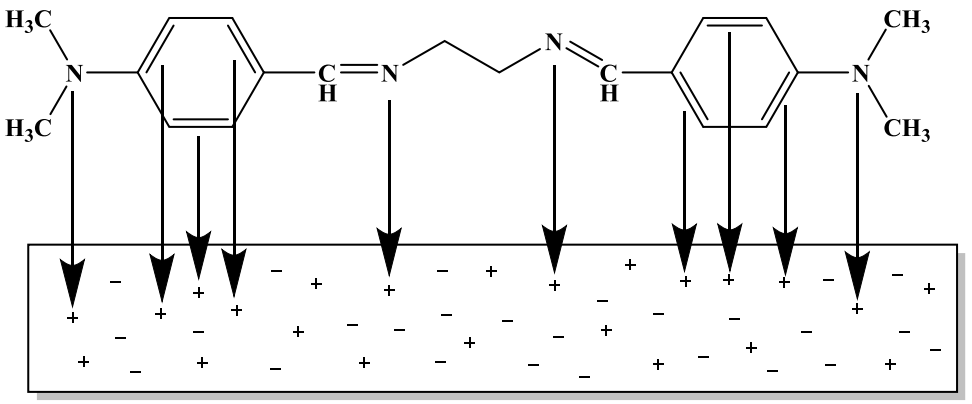

**Figure 9.** Schematic diagram representing adsorption of DMAB on the C-steel surface in 1.0 M HCl.

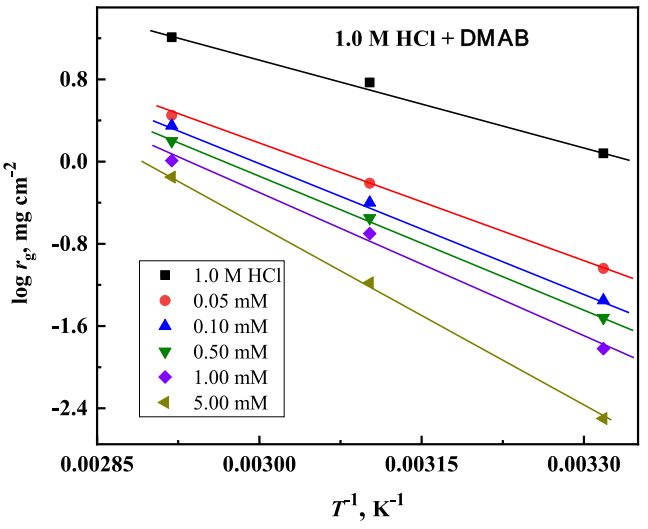


**Figure 10.** Arrhenius plots (log $k$ vs $1/T$) for the DMAB Schiff base compound on C-steel in 1.0 M HCl.

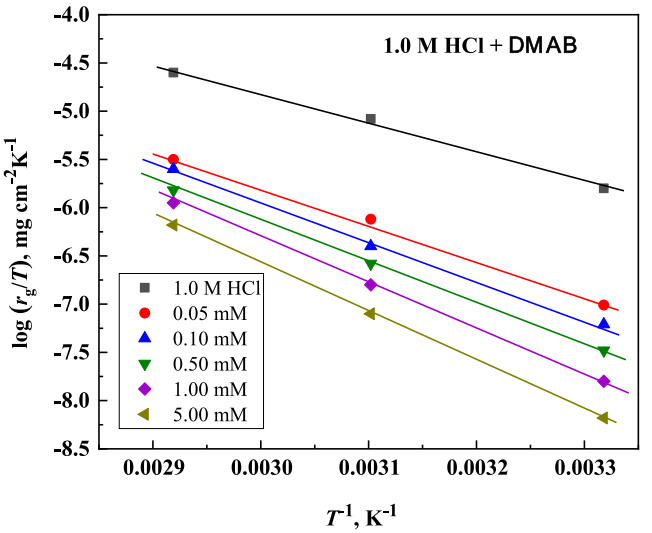


**Figure 11.** Transition state plots of ln $k/T$ versus $1/T$ for the corrosion of C-steel in 1.0 M HCl solution without and with different amounts of the DMAB compound.

**Table 9. Activation Thermodynamic Functions for C-Steel in Dilute Hydrochloric Acid Solutions Free of and Mixed with Various Amounts of the DMAB Compound**

| conc. of DBDB (mM) | $E_a$ (kJ mol$^{-1}$) | $\Delta H^*_{ads}$ (kJ mol$^{-1}$) | $\Delta S^*_{ads}$ (J mol$^{-1}$ K$^{-1}$) |
|---|---|---|---|
| 0.000 | 24.56 | 21.92 | −26.66 |
| 0.05 | 36.10 | 33.47 | −51.16 |
| 0.10 | 35.70 | 33.06 | −53.92 |
| 0.50 | 38.07 | 35.43 | −56.97 |
| 1.00 | 41.38 | 38.74 | −65.15 |
| 5.00 | 48.23 | 45.60 | −83.87 |

Also, the values of the thermodynamic functions $\Delta S^*$ and $\Delta H^*$ for different additions of the DMAB can be computed via the equation:[32]

$$\log(r_g T^{-1}) = \log\left(\frac{R}{N_A h}\right) + \left(\frac{\Delta S^*}{2.303R}\right) - \left(\frac{\Delta H^*}{2.303RT}\right) \quad (25)$$

where $N_A$ and $h$ refer to Avogadro's and Planck's constant, respectively. Figure 11 depicts the plotting of the log ($r_g$ $T^{-1}$) with $T^{-1}$ for all of the examined aggressive and inhibitive solutions. Such plots give straight line relationships with slopes = $-\Delta H^*/R$. The computed values of $\Delta H^*$ are listed in Table 9 and have a positive sign that explains the endothermic nature of the transition state accompanied by the corrosion inhibition process.[38,62] The values of $-\Delta S^*$ can be computed from the $y$-axis intercept of Figure 11 and computed to be 26.70 J mol$^{-1}$ K$^{-1}$ with dilute hydrochloric acid solution and vary from 51.2 to 83.9 J mol$^{-1}$ K$^{-1}$ with various amounts of the DMAB inhibitor, Table 9. The increase in the negativity of $\Delta S^*$ with more additions of the DMAB inhibitor would indicate that the activated complex in the rate-determining process represents an association rather than dissociation.[63−,11]

**3.10. Surface Investigation.** The morphology of the surface of some of the corroded and noncorroded metallic surfaces was investigated using SEM, complemented by the EDS analysis. Figures 12 and 13 depict the SEM and EDS analysis of three different samples of C-steel, respectively. The morphology of the surface of a clean and dry steel specimen, not exposed to any corrosive or inhibitive solution, is depicted in Figure 12A. The surface appeared to be smooth without any signs of corrosion, only occasional scratches resulting from polishing operations. Figure 12B depicts the morphology of the surface of the steel specimen after being offered into dilute HCl media for 4 h. Such a micrograph explains that the steel surface has several pits surrounded by corrosion products accommodated on the corroded metallic surface. The appearance of the highly destructive surface is owing to the



https://doi.org/10.1021/acsomega.4c03135
ACS Omega 2024, 9, 29666−29681

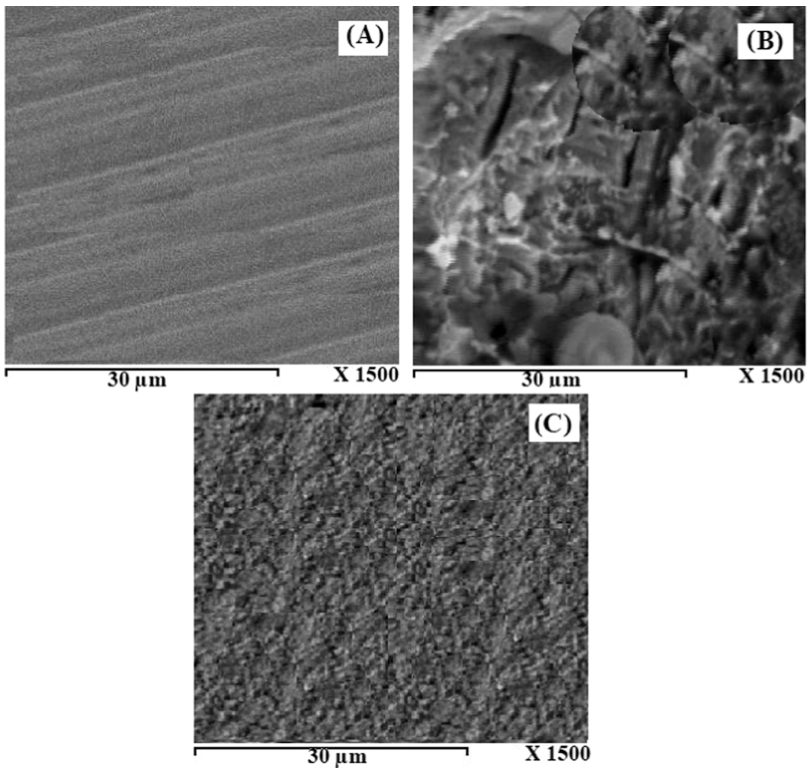


**Figure 12.** SEM micrographs of (A) carbon steel surface, (B) carbon steel in 1.0 M HCl devoid of, and (C) containing 0.005 M EDDB inhibitor at 25 °C.

presence of the corrosive chloride ions, which destroy the metallic surface in the absence of the DMAB inhibitor. Such a sample was analyzed to indicate a low value of Fe % in its metallic surface due to its dissolution in dilute HCl solution (1.0 M), Figure 13B. Figure 12C shows the SEM micrograph of the steel surface being offered for 4 h into a dilute hydrochloric acid containing 5 mM DMAB inhibitor. The micrograph explains the less corroded surface with corrosion products spreads on the metallic surface, owing to the existence of DMAB molecules that resist the corrosive influence of HCl by an adsorption process. In the EDS analysis of the metallic steel surface after exposing it to the hydrochloric acid containing the DMAB inhibitor, the Fe % appears to become greater than that of the free acid solution (Figure 13B), suggesting that the steel surface is covered by DMAB, so, the percent of iron loss into the HCl solution becomes lowered (Figure 13C).

**3.11. Quantum Computations.** *3.11.1. DFT Computations.* DFT calculations are utilized to examine the activity of the DMAB inhibitor to adsorb on the corroded metal. Figure 14 illustrates the optimized geometry of the DMAB compound with constant quantum parameters depicted in Table 10. Frontier molecular orbital, FMO, provides acquaintance about the activity of the DMAB molecules. The active centers that provide electrons to the surface of corroded steel are in the HOMO. On the other hand, the LUMO can institute feedback links by taking electrons from the investigated metal surface. The FMO distributions are shown in Figure 15.

The investigated DMAB substance has a little $\Delta E_g$ and a high $\sigma$ that confirms the high activity toward the adsorption on the examined metal surface.[66,67] Furthermore, molecules with a low $\sigma$ and a high $\Delta E$ are considered indicators of the high stability of such molecules. The higher $E_{HOMO}$ values sustain the investigated substance to donate $e^-$ to the active sites on the Fe surface with vacant d orbitals. The larger the $E_{HOMO}$ value, the higher the reactivity of such substance to share with $e^-$ on the examined metal surface. Moreover, $E_{LUMO}$ with a low value raises the probability of such substance accepting electrons, increasing the protection capacity. $\Delta E_g$ is a useful parameter in the reactivity of the DMAB compound to be adsorbed on the surface of the iron metal. The smaller $\Delta E_g$ value, the increases in the capability of the investigated DMAB substance to adsorb on the examined C-surface steel, Table 10.

A substance that has a small softness value, $\sigma$, and a high energy gap value, $\Delta E_g$, becomes confidently stable. A severe molecule that has a wide value of the energy gap, $\Delta E_g$, is considered less stable than a soft one with a cramped $\Delta E_g$. The substance with high global softness (lowest global hardness) is prophesied to have an excellent protection influence on the damaged metal surface[68] (Table 10).

The MEP, molecular electrostatic potential map, is predominantly accompanied by nucleophilic and electrophilic active sites located in the DMAB compound. The centers that appeared with a blue color in Figure 16 postulate the +ve sites while those with a red color assume the −ve regions located on the *N*-atom, designating the active centers on the adsorbed DMAB molecule.

The protection efficacy can be influenced by electron transfer, $e^-$. The $\Delta N$ deducts the transfer of $e^-$ from the examined surface of C-steel to the DMAB compound if $\Delta N$ is $< 0$ and from the inhibiting molecules to the surface of C-steel if $\Delta N$ is $> 0$.[69,70] The quantum computation data collected in Table 10 indicates that the electron transfer, $\Delta N$, is equal to 0.42 e with a positive value. Such data emphasizes that $\Delta N$ occurs from the DMAB molecule into the iron atom on the metallic surface. Such behavior proves that the theoretical


https://doi.org/10.1021/acsomega.4c03135
ACS Omega 2024, 9, 29666−29681

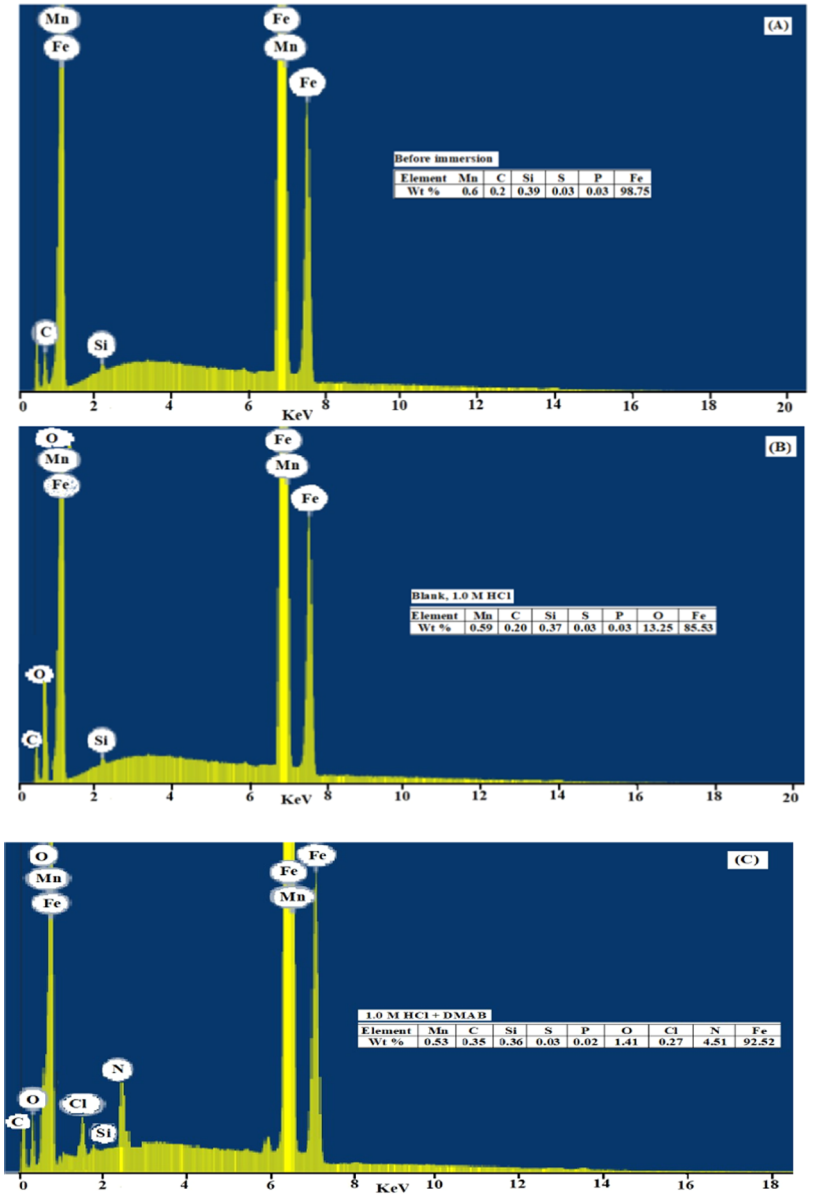


**Figure 13.** EDX spectra of (A) carbon steel surface, (B) carbon steel in 1.0 M HCl devoid of, and (C) containing 0.005 M DMAB inhibitor at 25 °C.

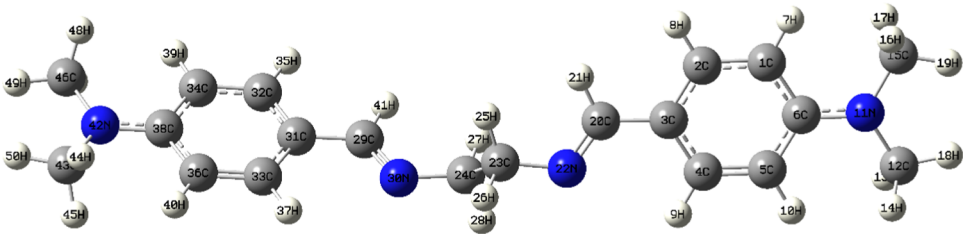

**Figure 14.** Optimized geometry of the DMAB Schiff base inhibitor.

**Table 10. Theoretical Quantum Functions of the DMAB Compound on C-Steel in Hydrochloric Acid Solution**

| $E_{HOMO}$, eV | $E_{LUMO}$, eV | $\Delta E$, eV | $\sigma$ ($eV^{-1}$) | $\eta$ (eV) | $\Delta N$ (e) |
|---|---|---|---|---|---|
| −5.16 | −0.89 | 4.27 | 0.47 | 2.135 | 0.42 |

computations are harmonious with the obtained experimental measurements.

The examined DMAB molecule in the acidic phase could be protonated owing to its chemical structure characterized by the presence of the heteroatom, nitrogen, which is rich with lone pairs of free electrons. Such atoms are active centers with high negative charges that make the DMAB compound be protonated easily. Figure 16 depicts the high negative charge centered on the N-atom of the dimethyl group in the DMAB compound and FMO of the optimized geometry of the DMAB



https://doi.org/10.1021/acsomega.4c03135
ACS Omega 2024, 9, 29666−29681

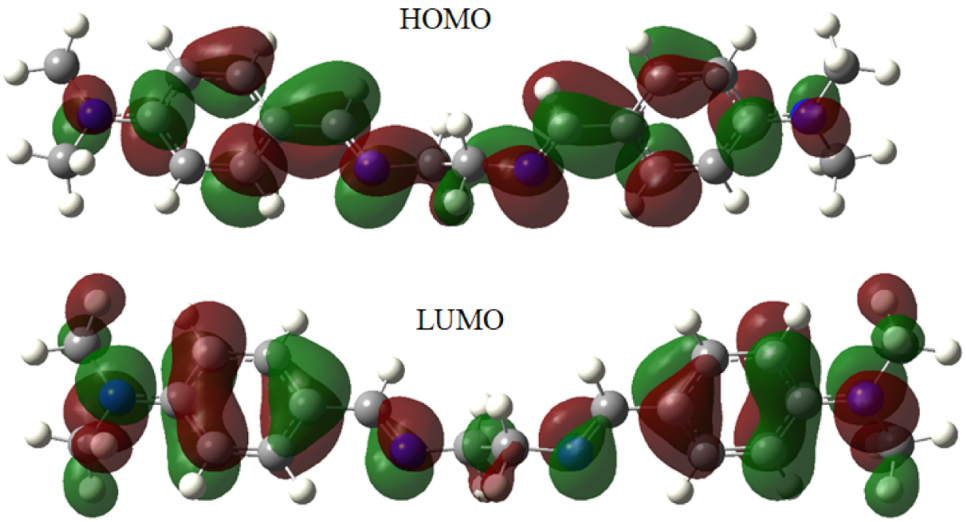


**Figure 15.** Frontier orbital, FMO, of the DMAB inhibitor.

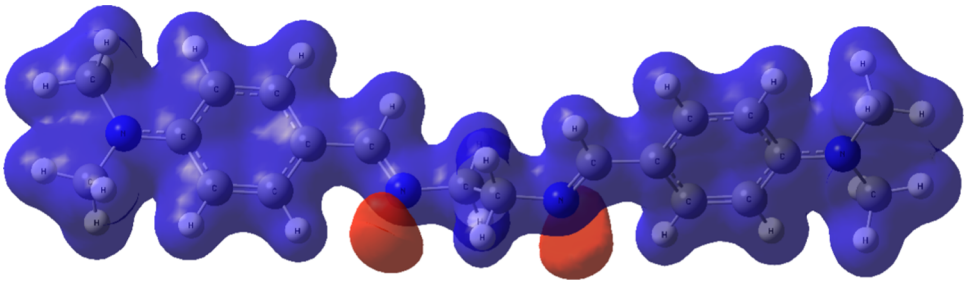

**Figure 16.** Molecular electrostatic map, MEP, of the DMAB inhibitor.

molecule. As explained in Figure 17, the FMO of the optimized geometry of the DMAB molecular, the $E_{HOMO}$ for the protonated DMAB substance is shifted to a more −ve value concerning the neutral $E_{HOMO}$. Such a situation explains the decrease in the $e^-$ donation of the DMAB compound molecule

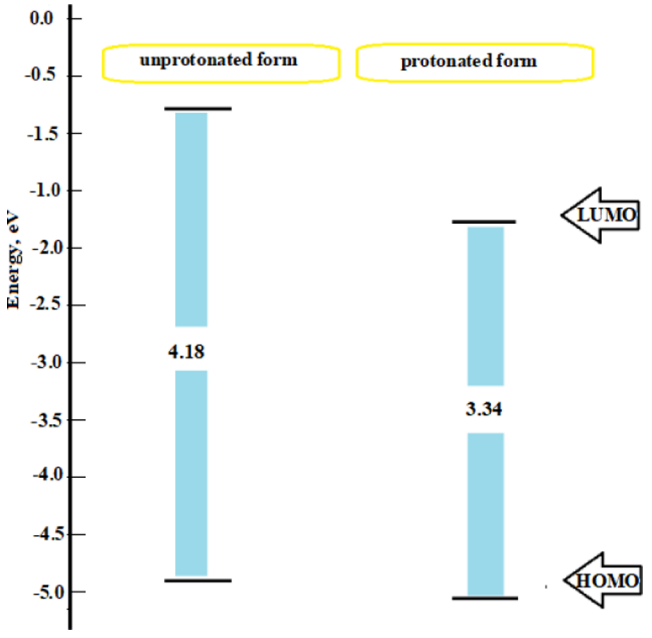


**Figure 17.** Frontier orbital energies of protonated and unprotonated forms for the DMAB Schiff base inhibitor.

to give $e^-$ to the metallic surface. The $E_{LUMO}$ value is shifted to a more -ve value than its neutral form, proving the capability to receive $e^-$ from the protonated one..

*3.11.2. Monte Carlo.* The Monte Carlo (MC) simulation proceeded to investigate the probability of the DMAB molecule reacting with the metallic surface of iron(110). The inhibitor molecules adsorb onto the Fe(110) surface in a nearly parallel way, covering the maximum surface area of the C-steel surface. This behavior is mostly attributed to the strong tendency of DMAB inhibitor compounds to donate electrons to vacant Fe orbitals and receive electrons from Fe d-orbitals via back-bonding[71,72] (Figure 18). Such orders of adsorption assume that the DMAB compound may be capable of donating and accepting $e^-$. The adsorption energy of the DMAB inhibitor molecule, $E$, is computed to be equal to −413.48 kcal $mol^{-1}$. Such data assume that the DMAB substance explains the high protection efficacy of the DMAB molecules against the corrosive effect of the chloride ions toward the metal surface, which comes in consistent with other practical data.

## 4. CONCLUSIONS

- The DMAB Schiff base compound was synthesized and assured by FTIR and mass spectroscopy.
- It behaves as an effective mixed-type inhibitor for the destruction of C-steel in 1.0 M HCl solutions.
- The gravimetry, gasometry, and electrochemical techniques were in good convention.
- The protection efficacy is found to be dependent on the inhibitor concentration and temperature.



https://doi.org/10.1021/acsomega.4c03135
ACS Omega 2024, 9, 29666−29681

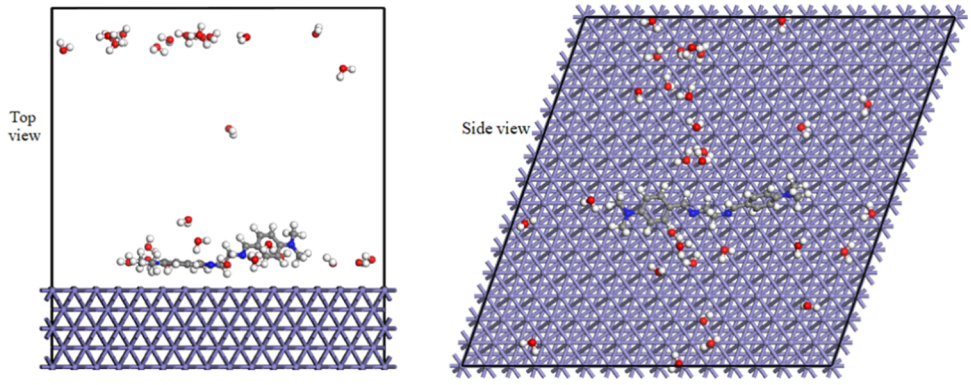


**Figure 18.** Top and side views of adsorption of the DMAB Schiff base inhibitor on the Fe(110) surface.

- The inhibition process was based on an adsorption mechanism obeying Langmuir's pattern.
- The reduction in the $\theta$ and the $\eta_w$ values with temperature could confirm the physisorption process.
- The large values of $K_{ads}$ confirm the strong adsorbability of DMBA on the C-steel surface.
- The negative value of $\Delta G^{\circ}_{ads}$ revealed the spontaneity of the adsorption process.
- The values of $\Delta G^{\circ}_{ads}$ and $\Delta H^{\circ}_{ads}$ confirm the adsorption of DMAB on the C-steel surface to be a chemisorption mechanism.
- Theoretical quantum computation confirmed the adsorption of DMAB in concurrence with the data obtained by practical techniques.

## AUTHOR INFORMATION


### Corresponding Authors

**Mahmoud G. Aboubakr Saleh** − *Department of Chemistry, College of Science, Northern Border University, Arar 91431, Saudi Arabia*; Email: mahmoud.saleh2@nbu.edu.sa

**Majda Alfakeer** − *Chemistry Department, College of Science, Princess Nourah Bint Abdulrahman University, Riyadh 11564, Saudi Arabia*; Email: msalonazi@pnu.edu

**Salah Abd El Wanees** − *Faculty College of Umluj, Umluj, University of Tabuk, Tabuk 47713, Saudi Arabia*; orcid.org/0000-0001-7099-5996; Email: s_wanees@yahoo.com

### Authors

**Rasha N. Felaly** − *Chemistry Department, Faculty of Science, Umm Al-Qura University, Makkah 24382, Saudi Arabia*

**Merfat S. Al-Sharif** − *Chemistry Department, College of Science, Taif University, Taif 21944, Saudi Arabia*

**Salih S. Al-Juaid** − *Chemistry Department, Faculty of Science, King Abdulaziz University, Jeddah 21589, Saudi Arabia*

**Kamal A. Soliman** − *Chemistry Department, Faculty of Science, Benha University, Benha 13518, Egypt*; orcid.org/0000-0001-8953-7709

**Mohamed A. Hegazy** − *Egyptian Petroleum Research Institute, Cairo 11727, Egypt*

**Sameer Nooh** − *Department of Information Systems, Faculty of Computing and Information Technology, King Abdulaziz University, Jeddah 21589, Saudi Arabia*

**Metwally Abdallah** − *Chemistry Department, Faculty of Science, Benha University, Benha 13518, Egypt; Chemistry Department, Faculty of Applied Science, Umm Al-Qura University, Makkah 24382, Saudi Arabia*; orcid.org/0000-0002-6132-8849

Complete contact information is available at: https://pubs.acs.org/10.1021/acsomega.4c03135


### Notes

The authors declare no competing financial interest.

## ACKNOWLEDGMENTS

(1) The authors extend their appreciation to the Deanship of Scientific Research at the Northern Border University, Arar, KSA, for funding this research work through the project number "NBU-FFR-2024-144-06". (2) The authors express their gratitude to Princess Nourah bint Abdulrahman University Researcher supporting project number (PNURSP2024R53) Princess Nourah bint Abdulrahman University, Riyadh, Saudi Arabia.

## REFERENCES

(1) Scendo, M. Inhibitive action of the purine and adenine for copper corrosion in sulfate solutions. *Corros. Sci.* **2007**, *49*, 2985−3000.

(2) Farag, A. A.; Migahed, M. A.; Al-Sabagh, A. M. Adsorption and inhibition behavior of a novel Schiff base on carbon steel corrosion in acid media. *Egypt J. Pet.* **2015**, *24*, 307−315.

(3) Finšgar, M.; Jackson, J. Application of corrosion inhibitors for steels in acidic media for the oil and gas industry: A review. *Corros. Sci.* **2014**, *86*, 17−41.

(4) Abdallah, M.; Zaafarany, I. A.; Abd El Wanees, S.; Assi, R. Breakdown of passivity of nickel electrode in sulfuric acid and its inhibition by pyridinone derivatives using the galvanostatic polarization technique. *Int. J. Corros. Scale Inhib.* **2015**, *4*, 338−352.

(5) Haleem, S. M. A. E.; Abd El Wanees, S.; Bahgat, A. Environmental factors affecting the corrosion behavior of reinforcing steel. VI. Benzotriazole and its derivatives as corrosion inhibitors of steel. *Corros. Sci.* **2014**, *87*, 321−333.

(6) Abdallah, M.; Zaafarany, I. A.; Abd El Wanees, S.; Assi, R. Corrosion behavior of nickel electrode in NaOH solution and its inhibition by some natural oils. *Int. J. Electrochem. Sci.* **2014**, *9*, 1071−1086.

(7) Al-Gorair, A. S.; Hawsawi, H.; Fawzy, A.; Sobhi, M.; Alharbi, A.; Hameed, R. S.; Abd El Wanees, S.; Abdallah, M. Evaluation of the anticorrosion and adsorption properties of polyethylene glycol and polyvinyl alcohol for corrosion of iron in 1.0 M NaCl solution. *Int. J. Electrochem. Sci.* **2021**, *16*, No. 211119.

(8) Abd El Wanees, S.; Alahmdi, M. I.; Rashwan, S. M.; Kamel, M. M.; Elsadek, M. G. A. Inhibitive effect of cetyltriphenylphosphonium bromide on C-steel corrosion in HCl solution. *Inter. J. Electrochem. Sci.* **2016**, *11*, 9265−9281.

(9) Al-Gorair, A. S.; Abd El Wanees, S.; Al-bonayan, A. M.; Al-Juaid, S. S.; Nooh, S.; Abdallah, M. Investigation of the effect of $ClO_4^-$ ions on the growth of indium oxide films on In electrode in dilute Na2B4O7 solution by potentiometric technique. *Int. J. Electrochem. Sci.* **2022**, *17*, No. 221251.
(10) Abd El Wanees, S.; Diab, A.; Azazy, O.; Azim, M. A. E. Inhibition effect of n-(pyridin-2-yl-carbamothioyl)benzamide on the corrosion of C-steel in sulfuric acid solutions. *J. Dispers. Sci. Technol.* **2014**, *35*, 1571−1580.
(11) Abd El Wanees, S.; Kamel, M. M.; Ibrahim, M.; Rashwan, S. M.; Atef, Y.; Elsadek, M. G. A. Corrosion inhibition and synergistic effect of ionic liquids and iodide ions on the corrosion of C-steel in formation water associated with crude oil. *J.Umm Al-Qura Univer. Appli. Sci.* **2023**, *10*, 107−119.
(12) Al-Gorair, A. S.; Saleh, M. G. A.; Alotaibi, M. T.; Al-Juaid, S. S.; Abdallah, M.; Abd El Wanees, S. Potentiometric and polarization studies on the oxide film repair and retardation of pitting corrosion on indium in an alkaline aqueous solution utilizing some triazole compounds. *Inorg. Chem. Commun.* **2023**, *158*, No. 111497.
(13) Hashim, N. Z. N.; Anouar, E. H.; Kassim, K.; Zaki, H. M.; Alharthi, A. I.; Embong, Z. XPS, and DFT investigations of corrosion inhibition of substituted benzylidene Schiff bases on mild steel in hydrochloric acid. *Appl. Surf. Sci.* **2019**, *476*, 861−877.
(14) Şahin, E. A.; Tezcan, F.; Solmaz, R.; Kardaş, G. Inhibitive effect of 4-amino-N-benzylidene-benzamide Schiff base on mild steel corrosion in HCl solution. *J. Adhes. Sci. Technol.* **2020**, *34*, 135−152.
(15) Betti, N.; Al-Amiery, A. A.; Al-Azzawi, W. K.; Isaha, W. N. R. W. Corrosion inhibition properties of Schiff base derivative against mild steel in HCl environment complemented with DFT investigations. *Sci. Rep.* **2023**, *13*, No. 8979.
(16) Zobeidi, A.; Nacer, S. N.; Atia, S.; Kribaa, L.; Kerassa, A.; Kamarchou, A.; Alnoaimi, M.; Ghernaout, D.; Ali, M. A.; Lagum, A. A.; Elboughdiri, N. Corrosion inhibition of Azo compounds derived from Schiff bases on mild steel (XC70) in (HCl, 1 M DMSO) medium: An experimental and theoretical study. *ACS Omega* **2023**, *8*, 21571−21584.
(17) Al-Gorair, A. S.; Abd El Wanees, S.; Hegazy, M. A.; Al-Juaid, S. S.; Soliman, K. A.; Asab, M. M. Experimental and theoretical studies on the corrosion inhibition on the surface of C-steel in hydrochloric acid solutions using $N^1$,$N^{1\prime}$-(ethane-1,2-diyl)bis($N^2$-(4-(dimethylamino)benzylidene)ethane-1,2 -diamine). *Mater. Chem. Phys.* **2023**, *297*, No. 127351.
(18) Al-Gorair, A. S.; Abd El Wanees, S.; Hawsawi, H. S.; Saleh, M. G. A.; Abdallah, M. Investigation of the anodic behavior of nickel in $H_2SO_4$ solutions using galvanostatic polarization technique. III. inhibition of pitting corrosion using nitrogen-containing organic compounds. *Desalin. Water Treat.* **2021**, *244*, 147−156.
(19) Boukazoula, S.; Haffar, D.; Bourzami, R.; Toukal, L.; Dorcet, V. Synthesis, characterizations, crystal structures, inhibition effects and theoretical study of novel Schiff base derived from hydroxynaphthaldehyde on the corrosion of carbon steel in 1 M HCl. *J. Mol. Struct.* **2022**, *1261*, No. 132852.
(20) Belghiti, M. E.; Benhiba, F.; Benzbiria, N.; Lai, C. H.; et al. Performance of triazole derivatives as potential corrosion inhibitors for mild steel in a strong phosphoric acid medium: combining experimental and computational (DFT, MDs & QSAR) approaches. *J. Mol. Struct.* **2022**, *1256*, No. 132515.
(21) Li, H.; Qiang, Y.; Zhao, W.; Zhang, S. A. Green brassica oleracea L extract as a novel corrosion inhibitor for Q235 steel in two typical acid media. *Colloids Surf., A* **2021**, *616*, No. 126077.
(22) Aal, E. E. A. E.; Abd El Wanees, S.; Farouk, A. A.; Haleem, S. M. A. E. Factors affecting the corrosion behavior of aluminum in acid solutions. II. Inorganic additives as corrosion inhibitors for Al in HCl solutions. *Corros. Sci.* **2013**, *68*, 14−24.
(23) Haleem, S. M. A. E.; Abd El Wanees, S.; Aal, E. E. A. E.; Farouk, A. Factors affecting the corrosion behavior of aluminum in acid solutions I. Nitrogen and/or sulfur-containing organic compounds as corrosion inhibitors for Al in HCl solutions. *Corros. Sci.* **2013**, *68*, 1−13.
(24) Abd El Wanees, S.; Saleh, M. G. A.; Hegazy, M. A.; Alahmdi, M. I.; Soliman, K. A.; Elsayed, N. H.; Abdelfatah, M.; Aljohani, M. M.; Nooh, S.; Asab, M.; Elyan, S. S. Mitigation of hydrogen production on C-steel in HCl solution using a benzylidene compound. *J. Adhes. Sci. Technol.* **2024**, *38*, 1161−1190.
(25) Abd El Wanees, S.; Seda, S. H. Corrosion inhibition of zinc in aqueous acidic media using a novel synthesized Schiff Base−an experimental and theoretical study. *J. Dispers. Sci. Technol.* **2019**, *40*, 1813−1826.
(26) Abd El Wanees, S.; Alahmdi, M. I.; Alsharif, M. A.; Atef, Y. Mitigation of hydrogen evolution during zinc corrosion in aqueous acidic media using 5-amino-4-imidazole- carboxamide. *Egypt. J. Chem.* **2019**, *62*, 811−825.
(27) Abdallah, M.; Soliman, K. A.; Alfakeer, M.; Hawsawi, H.; Al-bonayan, A. M.; Al-Juaid, S. S.; Abd El Wanees, S.; Motawea, M. S. Expired antifungal drugs as effective corrosion inhibitors for carbon steel in 1 M HCl solution: Practical and theoretical approaches. *ACS Omega* **2023**, *8*, 34516−34533.
(28) Abd El Wanees, S.; Basiony, N. M. E.; Al-Sabagh, A. M.; Alsharif, M. A.; Haleem, S. M. A. E.; Migahed, M. A. Controlling of $H_2$ gas production during Zn dissolution in HCl solutions. *J. Mol. Liq.* **2017**, *248*, 943−952.
(29) Kord, L.; Nasr-Esfahani, M. Corrosion behavior of carbon steel in HCl solution by Fe and Cr complexes with a Schiff-base ligand derived from salicylaldehyde and 2-(2-aminoethylamino)ethanol. *Surf. Eng. Appl. Electrochem.* **2015**, *51*, 491−500.
(30) Abdallah, M.; Al-Fahemi, J. H.; Soliman, K. A.; Al-Gorair, A. S.; Al-Sharif, M. S.; Al-Juaid; Abd El Wanees, S.; Sobhi, M. Exploring cinnamon extract's potential as a green corrosion inhibitor for X65 carbon steel in sulfuric acid: a comprehensive investigation. *J. Dispersion Sci. Technol.* **2024**, 1.
(31) Ahamad, I.; Prasad, R.; Quraishi, M. Adsorption and inhibitive properties of some new Mannich bases of isatin Derivatives on corrosion of mild steel in acidic media. *Corros. Sci.* **2010**, *52*, 1472−1481.
(32) Barone, V.; Cossi, M. Quantum calculation of molecular energies and energy gradients in solution by a conductor solvent model. *J. Phys. Chem. A.* **1998**, *102*, 1995−2001.
(33) Frisch, M. J.et al. *Gaussian 16*, Rev. C.01; Wallingford, CT 2016.
(34) Fouda, A. S.; Rashwan, S.; Emam, S.; El-Morsy, F. E. Corrosion inhibition of zinc in acid medium using some novel organic compounds. *Int. J. Electrochem. Sci.* **2018**, *13*, 3719−3744.
(35) Haleem, S. M. A. E.; Abd El Wanees, S.; Bahgat, A. Environmental factors affecting the corrosion behavior of reinforcing steel. V. Role of chloride and sulfate ions in the corrosion of reinforcing steel in saturated $Ca(OH)_2$ solutions. *Corros. Sci.* **2013**, *75*, 1−15.
(36) Abd El Wanees, S.; Al-Gorair, A. S.; Hawsawi, H.; Elyan, S. S.; Abdallah, M. Investigation of anodic behavior of nickel in $H_2SO_4$ solutions using galvanostatic polarization technique. II. Initiation and inhibition of pitting corrosion by some inorganic passivators. *Int. J. Electrochem. Sci.* **2021**, *16*, No. 210548.
(37) Alfakeer, M.; Abd El Wanees, S.; Hawsawi, H.; Al-Juaid, S. S.; Al-bonayan, A. M.; Abdallah, M.; Elyan, S. S. Controlling the oxide film destruction, metal dissolution, and $H_2$ generation on Al in acid solutions. *Desalin. Water Treat.* **2023**, *290*, 56−70.
(38) Fouda, A. S.; Ismail, M. A.; Abou-Shahbaz, R. M.; Husien, W. A.; El-Habab, E. S.; Abousalem, A. S. Experimental and computational chemical studies on the cationic furanylnicotinamidines as novel corrosion inhibitors in aqueous solutions. *Chin. J. Chem. Eng.* **2020**, *28*, 477−491.
(39) Li, W-h.; He, Q.; Zhang, S-t.; Pei, C-l.; Hou, B. R. Some new triazole derivatives as inhibitors for mild steel corrosion in acidic medium. *J. Appl. Electrochem.* **2008**, *38*, 289−295.
(40) El Azhar, M.; Mernari, B.; Traisnel, M.; Bentiss, F.; Lagrenee, M. Corrosion inhibition of mild steel by the new class of inhibitors [2,5-Bis(n-pyridyl)-1,3,4-thiadiazoles] in acidic media. *Corros. Sci.* **2001**, *43*, 2229−2238.


https://doi.org/10.1021/acsomega.4c03135
*ACS Omega* 2024, 9, 29666−29681

(41) Hamdy, A.; El-Gendy, N. S. Thermodynamic, adsorption, and electrochemical studies for corrosion inhibition of carbon steel by henna extract in acid medium. *Egypt. J. Petrol.* **2013**, *22*, 17−25.
(42) Deng, S.; Li, X.; Xie, X. Hydroxymethyl urea and 1,3-bis(hydroxy- methyl)urea as corrosion inhibitors for steel in HCl solution. *Corros. Sci.* **2014**, *80*, 276−289.
(43) Hegazy, M. A.; Abdallah, M.; Awad, M. K.; Rezk, M. Three novel di-quaternary ammonium salts as corrosion inhibitors for API X65 steel pipeline in acidic solution. Part I: Experimental results. *Corros. Sci.* **2014**, *81*, 54−64.
(44) Elseoud, W. S. A.; Abd-Karim, A. M.; Hassan, E. A.; Hassan, M. L. Enzyme- and acid-extracted sugar beet pectin as green corrosion inhibitors for mild steel in hydrochloric acid solution. *Carbohydr. Polym. Technol. Appl.* **2021**, *2*, No. 100072.
(45) Saleh, M. G. A.; Abd El Wanees, S. 2,2′-Dithiobis(2,3-dihydro-1,3-benzothiazole) as an effective inhibitor for carbon steel protection in acid solutions. *Desalin. Water Treat.* **2022**, *256*, 242−252.
(46) Sakunthala, P.; Vivekananthan, S. S.; Gopiraman, M.; Sulochana, N.; Vincent, A. R. Spectroscopic investigations of physicochemical interactions on mild steel in an acidic medium by environmentally friendly green inhibitors. *J. Surfactants Deterg.* **2013**, *16*, 251−263.
(47) Singh, A. K.; Chugh, B.; Singh, M.; Thakur, S.; Pani, B.; Guo, L.; Kaya, S.; Serdaroglu, G. Hydroxy phenyl hydrazides and their role as corrosion impeding agent: A detailed experimental and theoretical study. *J. Mol. Liq.* **2021**, *330*, No. 115605.
(48) Abd El Wanees, S.; Nooh, S.; Farouk, A.; Haleem, S. M. A. E. Corrosion inhibition of aluminum in sodium hydroxide solutions using some inorganic anions. *J. Dispers. Sci. Technol.* **2022**, *43*, 2021−2036.
(49) Alatalhi, A. A. Anticorrosion investigation of new diazene-based Schiff base derivatives as safe corrosion inhibitors for API X65 steel pipelines in acidic oilfield formation water: Synthesis, experimental, and computational studies. *ACS Omega* **2023**, *8*, 31271−31280.
(50) Chugh, B.; Singh, A. K.; Thakur, S.; Pani, B.; Lgaz, H.; Chung, I.-M.; Jha, R.; Ebenso, E. E. Comparative investigation of corrosion-mitigating behavior of thiadiazole-derived Bis-Schiff bases for mild steel in acid medium: Experimental, Theoretical, and Surface Study. *ACS Omega* **2020**, *5*, 13503−13520.
(51) Bockris, J.O'M.; Reddy, A.K.N.; Gamboa-Aldeco, M. *Modern Electro-chemistry*, 2nd ed.; Kluwer Academic/Plenum Publishers: New York, 2000.
(52) Saleh, M. G.; Abd El Wanees, S.; Mustafa, S. K. Dihydropyridine derivatives as controllers for the production of hydrogen during zinc dissolution. *Chem. Eng. Commun.* **2019**, *206*, 789−803.
(53) Mazumder, M. A. J. Synthesis, characterization, and electrochemical analysis of cysteine modified polymers for corrosion inhibition of mild steel in aqueous 1 M HCl. *RSC Adv.* **2019**, *9*, 4277−4294.
(54) Badawi, A.; Hegazy, M. A.; El-Sawy, A.; Ahmed, H.; Kamel, W. Novel quaternary ammonium hydroxide cationic surfactants as corrosion inhibitors for carbon steel and as biocides for sulfate-reducing bacteria (SRB). *Mater. Chem. Phys.* **2010**, *124*, 458−465.
(55) Alharthi, N. H.; El-Hashemy, M. A.; Derafa, W. M.; Althobaiti, I. O.; Altaleb, H. A. Corrosion inhibition of mild steel by highly sable polydentate Schiff base derived from 1,3-propane diamine in aqueous acidic solution. *J. Saudi. Chem. Soc.* **2022**, *51*, 1935−1949.
(56) Moretti, G.; Guidi, F.; Grion, G. Tryptamine as a green iron corrosion inhibitor in 0.5 M deaerated sulphuric acid. *Corros. Sci.* **2004**, *46*, 387−403.
(57) Scend, M.; Trela, J. Corrosion inhibition of carbon steel in acid chloride solution by Schiff base of n-(2-chloro benzylidene)-4-acetylcholine. *Int. J. Electrochem. Sci.* **2013**, *8*, 8329−8347.
(58) Al-Gorair, A. S.; Al-Sharif, M. S.; Al-Juaid, S. S.; Saleh, M. G. A.; Abdelfattah, M.; Abdallah, M.; Abd El Wanees, S. Bis(2-hydroxyethyl) ammonium dodecanoate and its constituents as inhibitors for Al corrosion and $H_2$ production in acid medium. *Int. J. Electrochem. Sci.* **2024**, *19*, No. 100452.
(59) Hussein, M. H. M.; El-Hady, M. F.; Shehata, H. A. H.; Hegazy, M. A.; Hefni, H. H. H. Preparation of some eco-friendly corrosion inhibitors having antibacterial activity from seafood waste. *J. Surfactant Deterg.* **2013**, *16*, 233−242.
(60) Al-Gorair, A. S.; Felaly, R. N.; Al-Sharif, M. S.; Al-Juaidd, S. S.; Saleh, M. G. A.; Abdallah, M.; Abd El Wanees, S. Inhibition of general and pitting corrosion of Ni in dilute sulfuric acid solutions utilizing some tetrazole derivatives. *Int. J. Electrochem. Sci.* **2024**, *19*, No. 100456.
(61) Abd El Wanees, S.; Abdallah, M.; Al-Gorair, A. S.; Tirkistani, F. A. A.; Nooh, S.; Assi, R. Investigation of anodic behavior of nickel in $H_2SO_4$ solutions using galvanostatic polarization technique. I. Kinetics and thermodynamic approach. *Int. J. Electrochem Sci.* **2021**, *16*, No. 150969.
(62) Karthik, R.; Muthukrishnan, P.; Chen, S-M.; Jeyaprabha, B.; Prakash, P. Anti-corrosion inhibition of mild steel in 1M hydrochloric acid solution by using tiliacora acuminate leaves extract. *Int. J. Electrochem. Sci.* **2015**, *10*, 3707−3725.
(63) Rehim, S. S. A. E.; Sayyah, S. M.; El-Deeb, M. M.; Kamal, S. M.; Azooz, R. E. Adsorption and corrosion inhibitive properties of p(2-aminobenzothiazole) on mild steel in hydrochloric acid media. *Int. J Ind. Chem.* **2016**, *7*, 39−52.
(64) Abd El Wanees, S.; Al-Gorair, A. S.; Hawsawi, H.; Alotaibi, M. T.; Saleh, M. G. A.; Abdallah, M.; Elyan, S. S. Inhibition of pitting corrosion of C-steel in oilfield-produced water using some purine derivatives. *Desalin. Water Treat.* **2022**, *269*, 21−32.
(65) Abd El Wanees, S.; Keshk, A. A. Investigation of anodic behavior of nickel in $H_2SO_4$ solutions using galvanostatic polarization technique. IV. Initiation and inhibition of pitting corrosion by $Cl^-$ ions and ethoxylated surfactants. *Int. J. Electrochem. Sci.* **2021**, *16*, 21087.
(66) Tan, B.; Zhang, S.; Qiang, Y.; Feng, L.; Liao, C.; Xu, Y.; Chen, S. Investigation of the inhibition effect of montelukast sodium on the copper corrosion in 0.5 mol/l $H_2SO_4$. *J. Mol. Liq.* **2017**, *248*, 902−910.
(67) Zheng, X.; Zhang, S.; Li, W.; Yin, L.; He, J.; Wu, J. Investigation of 1-butyl-3-methyl-1H-benzimidazolium iodide as an inhibitor for mild steel in sulfuric acid solution. *Corros. Sci.* **2014**, *80*, 383−392.
(68) Ebenso, E. E.; Isabirye, D.; Eddy, N. O. Adsorption, and quantum chemical studies on the inhibition potentials of some thiosemicarbazides for the corrosion of mild steel in acidic medium. *Inter. J. Mol. Sci.* **2010**, *11*, 2473−2498.
(69) Kokalj, A.; Kovačević, N. On the consistent use of electrophilicity index and HSAB-based electron transfer and its associated change of energy parameters. *Chem. Phys. Lett.* **2011**, *507*, 181−184.
(70) Abd El Wanees, S.; Saleh, M. G. A.; Elsayed, N. H.; Aljohni, M. M.; Abdelfattah, M.; Soliman, K. A.; Alahmdi, M. I.; Alalati, M. L.; Elyan, S. S. Benzimidazole-modified chitosan as a controller for the destruction of Al and $H_2$ generation in the acidic environment. *Mater. Chem. Phys.* **2024**, *311*, No. 128484.
(71) Qiang, Y.; Li, H.; Lan, X. Self-assembling anchored film basing on two tetrazole derivatives for application to protect copper in sulfuric acid environment. *J. Mater. Sci. Technol.* **2020**, *52*, 63−71.
(72) Qiang, Y.; Zhang, S.; Yan, S.; Zou, X.; Chen, S. Three indazole derivatives as corrosion inhibitors of copper in a neutral chloride solution. *Corros. Sci.* **2017**, *126*, 295−304.


https://doi.org/10.1021/acsomega.4c03135
*ACS Omega* 2024, 9, 29666−29681